

Summer Wind-Driven Near-Inertial Oscillations in the Continental Shelf off Concepción, Chile.

Claudio Iturra^{1,2}, Marcus Sobarzo¹, John Largier³.

¹Department of Oceanography, University of Concepción.

²Graduate Program in Oceanography, University of Concepción.

The presented manuscript is part of the author's graduate education in the Graduate Program in Oceanography at the University of Concepción, Chile. Initially, the data analysis was conducted using Matlab; however, the second version of the manuscript data analysis was entirely re-written using Python and Julia.

Corresponding author : claudioiturra@oceanografia.udec.cl

Credit Authorship Contribution Statement: Claudio Iturra: Writing (original draft and review/editing), validation, investigation, data analysis, and image generation. Marcus Sobarzo: John Largier.

Abstract

This study explores the dynamics of Near-Inertial Oscillations (NIOs) in the coastal ocean during the summer of January 2005, focusing on their temporal and spatial characteristics at the coastal location of Concepcion. The analysis reveals NIOs as the predominant frequency in the negative rotary spectra of the first baroclinic mode of horizontal velocities, accounting for 63% of the total current variance from 5 to 90 meters depth. Observations indicate that NIOs begin to significantly influence current patterns below 5 meters, where currents transition from wind-driven to anticlockwise rotary motions due to the Coriolis effect. The vertical distribution and decay of NIOs are closely linked to the thermal structure of the ocean, with stronger stratification during upwelling relaxation events facilitating deeper penetration of NIOs, while weaker stratification during upwelling events confines them to shallower depths. The study also examines the interaction between NIOs and sub-inertial currents, showing that weak sub-inertial flows promote stronger and more persistent NIO rotary motions, whereas stronger flows lead to accelerated decay and deformation of these oscillations. Local wind patterns, particularly intensified diurnal winds associated with sea breezes, are identified as key drivers for NIO generation. The Sea Breeze Index (SBI) calculated highlights periods conducive to sea-breeze formation, which correlate with enhanced NIO activity. The interaction between locally generated and advected NIOs at L1 is explored through spectral analysis and simulations, revealing processes like superposition and a form of pseudo-resonance that can either amplify or dampen NIO velocities. Finally, the impact of NIOs on biological productivity is assessed through vertical profiles of physical and biological properties, demonstrating how NIOs affect oxygen levels, stratification, and nutrient distribution, thereby modulating primary productivity. This comprehensive study underscores the complex interplay between physical oceanographic processes and biological responses, providing insights into the role of NIOs in coastal ocean dynamics during summer conditions.

Keywords : NIOs, Mixing, Baroclinic, Shear of Turbulence, Upwelling, Relaxation.

Introduction

Spatial and temporal variability of winds over the surface ocean induce circulation across a wide range of frequencies, strongly controlling coastal ocean dynamics (physical, chemical, and biological aspects of coastal environments). A key oceanic variability induced by winds over the upper ocean layers are the Near-Inertial motions (NIMs), well-represented as the most prominent and significant energy peak in the Garrett and Munk (1975) internal wave spectrum. Near-inertial motions have been observed and described since Ekman (1953), followed by Webster (1968), and have been reported globally throughout the ocean (Alford et al. 2016). These motions are oceanic currents that oscillate at frequencies close to the local inertial frequency (f_i), which is determined by Earth's rotation and latitude. The primary manifestation of Near-Inertial Motions (NIMs) are Near-Inertial Oscillations (NIOs), characterized by circularly polarized horizontal velocities and typically generated by local wind forcing (Alford et al. 2016; S. Chen, Chen, and Xing 2017; Pollard and Millard 1970). Most of the initial near-inertial energy from NIOs in the mixed layer leaves the forcing region through downward (radiate downward) and lateral propagation, as well as turbulent dissipation, with downward propagation being the primary mechanism for transferring energy from the mixed layer to the deeper ocean. (Alford 2020; Alford et al. 2016; D'Asaro 1989; Johnston et al. 2016; S. Chen, Chen, and Xing 2017; Cyriac et al. 2022; Song et al. 2021). The downward traveling of NIOs into the stratified ocean below the mixed layer depth can lead to Near-Inertial internal waves (NIWs). NIWs are similar to NIOs but propagate along density interfaces and have a slightly higher frequency due to the influence of stratification. Both NIOs and NIWs are important for understanding the transfer of mechanical energy to the ocean by the surface wind, its loss to the internal wave field, and eventual dissipation. The slab model, described by Pollard and Millard (1970), has been used to quantify the Near-Inertial energy transferred from wind to the upper ocean and thus available for downward propagation. Global estimation suggest that the wind power input to near-inertial motions in the surface mixed layer depth is estimated to be around 0.3-0.6 TW (Flexas et al. 2019; Watanabe and Hibiya 2002; Liu, Jing, and Wu 2019). The amount of wind-power to Near-inertial motions is comparable in magnitude to the power impute of geostrophic flow and internal tides (Alford 2003), suggesting the wind induced near-inertial motions are an important component of the ocean's energy budget.

Multiple factors, including the strength and duration of wind forcing (diurnal winds and storms), ocean stratification, mixed layer depth, coastal fronts, and background currents (e.g., sub-inertial circulation-upwelling, vorticity, eddies), influence the propagation and decay of near-inertial motions (NIMs) along the water column (Johnston et al. 2016; S. Chen, Chen, and Xing 2017). In regions with weaker stratification, NIOs can propagate more freely to deeper depths, easily reaching the pycnocline and penetrating into the deep ocean. The weaker stratification facilitates the efficient transfer of near-inertial energy from the surface to the deeper ocean, preserving the vertical structure of NIOs and inducing mixing (Shengli Chen et al. 2019). Conversely, with strong stratification, NIOs tend to be trapped near the surface, preventing energy from reaching deeper depths. The vertical structure of NIOs can be significantly modified by strong stratification, leading to vertically compressed waves that could trigger mixing due to strong shear in the upper ocean (Alford 2020).

While Near-Inertial Oscillations (NIOs) and Near-Inertial Waves (NIWs) have been extensively studied in the open ocean, their behavior in coastal regions, particularly within Eastern Boundary Upwelling Systems (EBUS), remains a complex and challenging area of research. Studies utilizing numerical simulations have shown that inertial oscillations can be predicted based on wind forcing and coastal bathymetry. Observational data often aligns with theoretical models, confirming that these oscillations play a crucial role in coastal ocean dynamics (Kelly 2019; Tintoré et al. 1995). Simulations of shelf near-inertial motions suggest that the horizontal distribution of Near-Inertial energy is primarily forced by Inertial Oscillations S. Chen, Chen, and Xing

(2017), which is the main interest of the presented research. Characteristic of NIOs over continental shelf, is the two layers structure, with opposite phase between surface and lower layer currents, mostly generated by the interaction of barotropic waves and inertial currents (Alford et al. 2016; Shengli Chen et al. 2019). The intensity of NIOs increases offshore, reaching its strongest velocities near the shelf break. The circulation resulting from the interaction between inertial motions and coastal features, such as tidal currents and sub-inertial motions, can create complex patterns of movement that significantly influence the vertical structure of the water column. This interaction can modify local Richardson numbers, potentially reducing them below a critical value and triggering mixing (Gregg 1989; Kunze, Briscoe, and Williams III 1990). Additionally, Submarine canyons and other coastal topographic features can significantly alter the structure and propagation of near-inertial motions over the continental shelf (Garrett and Munk 1975; Alford et al. 2016; Xing and Davies 2004).

Wind-induced near-inertial oscillations (NIOs) were investigated over the continental shelf, approximately 20 kilometers offshore from the coast of Concepción, in central-southern Chile, during the summer of 2005. During this period, the coastal waters off south-central Chile were characterized by upwelling circulation, relaxation events, strong thermal fronts, eddies, and shallow water dynamics (Arcos and Wilson 1984; Sobarzo and Djurfeldt 2004). The southerly upwelling-favorable winds during the summer brought nutrient-rich, low-oxygen waters to the surface, enhancing primary productivity in the region (Escribano and Schneider 2007; Escribano et al. 2007). The wind-induced circulation around the study area is strongly influenced by seasonal, synoptic, and diurnal wind patterns. This research focuses on the diurnal fluctuations of the wind and their potential to induce strong inertial motions that radiate across the thermocline. Diurnal wind variability over the continental shelf of Concepción is significantly intensified by the local sea breeze, which generates a cross-shore pressure gradient, driving strong onshore winds during the day and inducing strong near-diurnal circulation (Sobarzo, Shearman, and Lentz 2007, 2007; Sobarzo, Bravo, and Moffat 2010; Aguirre, Pizarro, and Sobarzo 2010). Over the continental shelf of Concepcion, the diurnal wind can force strong baroclinic currents, where near-inertial motions can account for up to 60% of the total current variability, depending on the location and time of year (Sobarzo, Shearman, and Lentz 2007). In the coastal region, the interaction between inertial motions, sub-inertial currents, tides, and internal waves is not yet fully understood. However, based on research in similar shelf environments, these interactions can significantly contribute to vertical mixing, with important ecological consequences for the area (Alford et al. 2016; Alford 2020).

Recent investigations in the central-south region of Chile and the eastern boundary current suggest an intensification of coastal stratification (Du et al. 2024; Oyarzún and Brierley 2018) and coastal hypoxia (De La Maza and Farías 2023; Farias and Maza 2024). Harmful algal blooms (HABs) are also intensifying globally, with the central coast of Chile experiencing an increase in both the frequency of HABs and their spatial variability (Barría et al. 2022; Du et al. 2024; Gobler 2020; Hallegraeff, Enevoldsen, and Zingone 2021; Dai et al. 2023; Griffith and Gobler 2020). Global estimates indicate that near-inertial oscillations (NIOs) are intensifying (Qian et al. 2023), and these motions can significantly influence the vertical mixing of coastal waters. This mixing facilitates the exchange of heat, nutrients, and gases between the surface and deeper layers, which may help moderate some of the impacts of climate change by redistributing heat and reducing surface ocean warming. Additionally, NIOs can enhance the upwelling of nutrient-rich waters, supporting marine ecosystems. However, while NIOs may offer some benefits, they can also exacerbate existing local conditions such as coastal hypoxia, increased stratification, altered coastal ventilation rates, and changes in local productivity. The enhanced retention of water masses caused by intensified NIOs could trap nutrients and pollutants near the coast, potentially leading to more severe and prolonged hypoxic events. The combined effects of climate change, local oceanographic conditions and intensified NIOs could pose significant risks to the region's marine ecosystems, fisheries, and aquaculture industries. Understanding the complex interplay between NIOs and these

coastal processes is crucial for developing effective mitigation and adaptation strategies to protect the marine environment and coastal communities in the face of a changing climate.

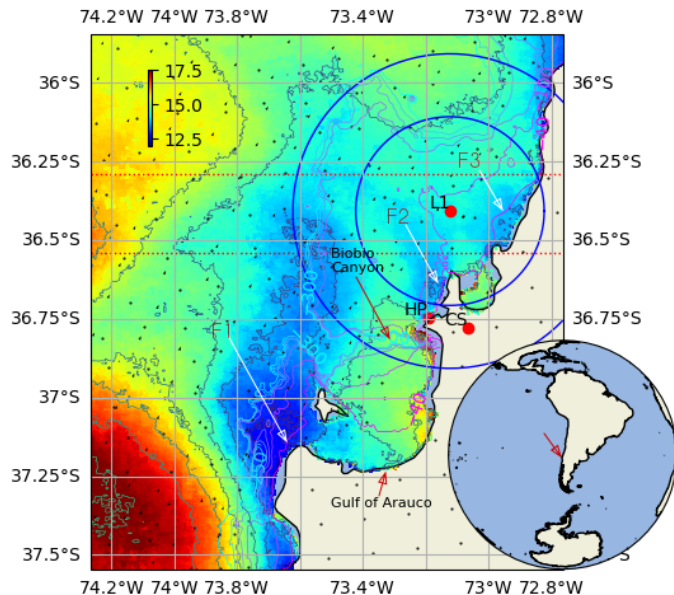


Figure 01: A detailed map of the study area on the continental shelf off Concepción, Chile, is presented. The map features mooring locations at L1, weather stations at CS and HP, and a surface buoy at P. Bathymetric contours of 40, 100, 150, 200, and 300 meters are delineated by colored lines, respectively. The map also visualizes the trajectories of two surface drifters (A and B) from the NOAA Global Drifter Program. These drifters exhibit clear Inertial Oscillations in their paths, particularly near the continental shelf break. Sea surface temperature climatology composite for January 2005 is represented by a color gradient. A prominent cold water plume is evident at Punta Lavapié, while two smaller cold plumes are observed in San Vicente Bay and Dichato. Black dots indicate the location/path of a single orbital revolution of the QuikSCAT satellite measuring surface winds over the study area. The un-gridded wind data inside the blue circle was averaged per orbital revolution to create an along-shore and cross-shore wind time series.

Methods

In January 2005, an oceanographic research expedition was conducted aboard the University of Concepción's research vessel, Kay-Kay II, off the continental shelf of central Chile. The expedition was centered 22 kilometers from the Bay of Concepción at location L1 (-36.4075°S, -73.122°W, see Figure 1), where the depth was approximately 100 meters. During the fieldwork, the horizontal current velocity of the water column was measured from 7 to 90 meters depth using a bottom-mounted ADCP (Acoustic Doppler Current Profiler). Simultaneously, another ADCP was mounted on a subsurface buoy at 55 meters depth to measure the upper ocean horizontal velocity above 50 meters, with a vertical resolution of 1 meter for a shorter period. Properties of the water column were evaluated using CTD profiles and a thermistor chain with temperature sensors ranging from 6 to 97 meters.

Pre-Evaluation of the Fieldwork Data

The bottom-mounted 300 kHz ADCP, deployed at a depth of ~100 meters, was programmed to measure current velocities every 30 minutes, with a standard bin size of 8 meters. This temporal resolution is sufficient to capture NIOs. Data from the upper 10 meters of the bottom-mounted ADCP were discarded due to poor quality and data gaps. In contrast, only the first 2 meters (2 bins) were removed from the high-resolution

vertical measurements obtained from the subsurface buoy-mounted ADCP, which measured horizontal velocities every 5 minutes with a bin size of 1 meter. The raw ADCP horizontal velocity data were decomposed into their eastward and northward components, preserving the 30-minute and 5-minute time resolutions of the respective data series. Minor gaps in the data were detected at specific depth levels. Multiple analyses were conducted on both the raw horizontal current velocities and the tidal residual velocities (baroclinic). The tidal signal was removed from the horizontal velocities using the python unified tidal analysis (UTide) by Codiga (2011), which performs harmonic analysis of ocean tides. A multitaper spectral analysis was employed to examine the dominant frequency variability and energy distribution of the horizontal velocities and sea-level height. Rotary spectral analysis was used to describe the dominant frequencies of clockwise and anticlockwise rotary trajectories. For non-bivariate data, such as temperature and sea-level time series, standard spectral analysis was used to identify dominant frequencies. Specific frequency bands were isolated from the time series using a Butterworth band-pass filter applied to the multiple temporal resolution time series. To prevent phase distortion in the filtered data, the filter was applied in both forward and backward directions.

Extracting Near-Inertial motions from current horizontal velocities

Extracting Near-Inertial Oscillations (NIOs) from horizontal current velocity data is particularly challenging in shallow coastal ocean systems around 30 degrees latitude, where significant energy exists near the local inertial frequency. The presence of diurnal energy from winds, tides, and shallow water components complicates the isolation of pure inertial velocities, which are also influenced by sub-inertial and super-inertial motions. In this research, NIOs will be extracted from the baroclinic current velocity signal using a one-sided narrow-band filter based on the wavelet transform. The wavelet transform has increasingly been utilized to isolate localized bands of variability, such as those associated with tides, NIOs, or internal waves. (Flinchem and Jay 2000; Lilly and Olhede 2010; Lilly 2017).

Inertial oscillations exhibit a counterclockwise rotation at a frequency close to the local Coriolis frequency. To investigate this phenomenon, we developed and validated a narrow-band filter utilizing the wavelet transform. This filter was designed to isolate the counterclockwise rotational velocity components centered around the local inertial frequency, enabling us to analyze the inertial rotary interaction between the alongshore and cross-shore current velocity components. The Morse filter, employed to extract near-inertial motions, is governed by three parameters: gamma, beta, and omega. Gamma dictates the filter's shape, beta determines its frequency bandwidth, and omega represents the central frequency. Figure 2, panels (a) and (b), illustrate the positive and negative rotary spectra of current velocity at a depth of 7 meters, highlighting the dominant rotary frequencies during January 2005. The green line in panel (b) represents the filter's output, selectively extracting energy associated with the near-inertial frequency peak from the counterclockwise frequencies. Panel (c) displays the temporal variations of the extracted near-inertial velocity, while panel (d) depicts its trajectory, forming a circular path with a nearly constant period of 20 hours. After testing the NIOs extraction method with both synthetic time series and in-situ current velocity data, we found that the narrow-band filter based on the wavelet transform provides a significantly better representation of near-pure inertial oscillations than the Butterworth filter applied to current velocities, resulting in an average accuracy improvement of 30%. The negative frequency residual spectra of the Butterworth filter time series velocity show a wider inertial frequency, taking energy from diurnal frequencies and affecting NIOs' fluctuations, inducing a dominant 5-day sub-inertial fluctuation in the velocity.

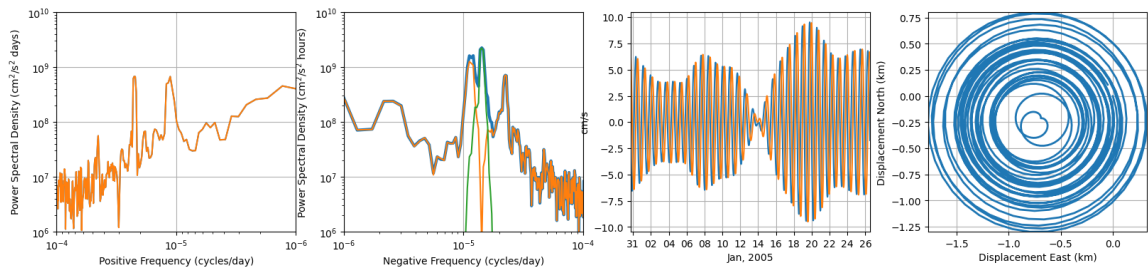


Figure 02: Panels (a) and (b) illustrate the positive (clockwise trajectories) and negative (anticlockwise trajectories) rotary spectra of the upper ocean current at a depth of 7 meters. In these panels, blue lines indicate the total velocity, orange lines represent the residual velocity after removing the near-inertial rotary motions, and the green line overlaid on the negative rotary spectra shows the extracted near-inertial oscillation (NIO) velocity. Panel (c) shows the temporal variability of the extracted near-inertial velocity, while panel (d) depicts the trajectory of the near-inertial current.

Coastal winds over the shallow shelf of Concepción and wind induced NIOs.

Evaluating the temporal and spatial variability of winds over the continental shelf of central Chile has historically been challenging due to the absence of buoy-based wind measurements and the complex atmospheric processes that modify coastal winds near the coast. In this study, we assess winds over the Concepción continental shelf using data from two weather stations: the coastal Hualpén (HP) station and the Carriel-Sur (CS) station, which is 15 kilometers inland. Data from these stations were obtained from the Dirección General de Aeronáutica Civil de Chile's website (meteochile.gob.cl).

Additionally, we utilized ungridded Level-2 satellite wind data from 60 QuikSCAT scatterometer orbits during January 2005 to analyze the spatial and temporal dynamics of the wind at location L1. Measurements were taken twice daily at 10-11 UTC and 22-23 UTC, with the data sourced from the Remote Sensing Systems website. For each orbit, wind direction and speed data were extracted within a 0.5-degree radius circle centered at L1 to construct time series of alongshore and cross-shore wind components. Furthermore, wind data from the ERA5 reanalysis were downloaded from the Copernicus Climate Data Store to create a time series of wind velocity near location L1. Results from all wind datasets are depicted in Figure 03.

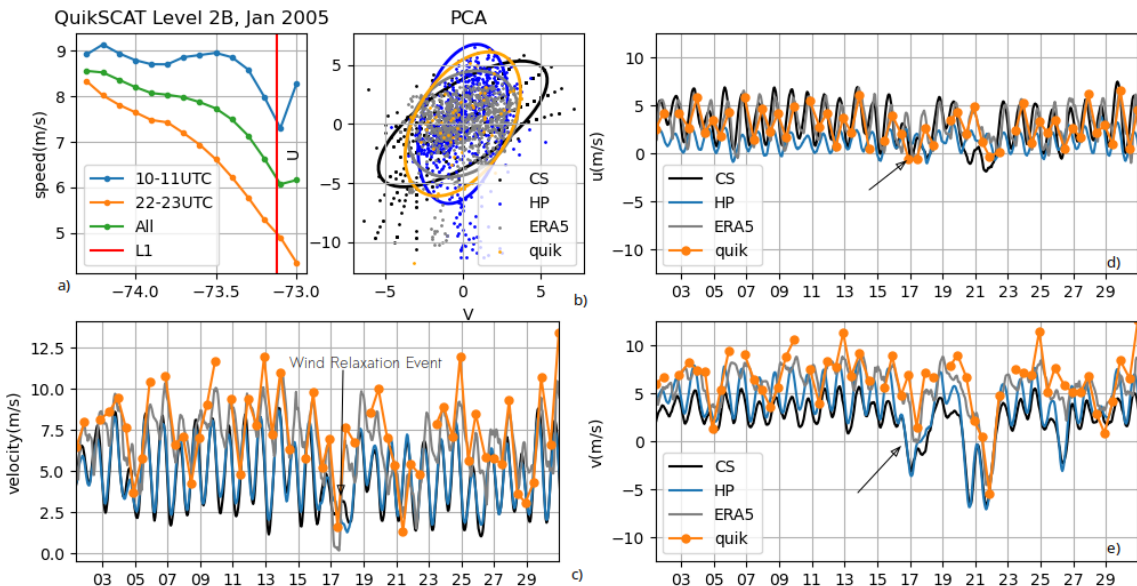


Figure 03. Panel (a). Displays the longitudinal average section of satellite wind velocity, averaged over 60 revolutions during Jan 2005, centered at location L1. It illustrates the durnal amplitude of the wind, which intensify toward the coast. Panel (b): Shows the ellipse

generated by the minor and major axes from Principal Component Analysis (PCA) for the wind data measured by the CS, HP, QuikSCAT satellites and ERA 5 Reanalysis wind. Panels (c) and (d): Depict the along-shore and cross-shore components of the wind measured by the CS, HP, QuikSCAT satellites, and ERA 5 Reanalysis wind respectively. Panel (e): Represents the total velocity of the wind data from the same sources as mentioned.

Recently, an oceanographic buoy named POSAR was installed on the shallow shelf of Concepción, near location L1. The buoy is equipped with multiple sensors, including an R.M. Young 05106 anemometer, which measures wind direction and velocity at 2 meters above sea level. Data transmission from the buoy started on August 22, 2024, marking the first instance of continuous wind measurements over the continental shelf, 25 kilometers offshore. After the first month of data collection, these measurements are being utilized to evaluate the accuracy of a historical wind database for the study area, specifically for the year 2005. Although the data collected did not correspond to the summer season, a strong diurnal wind amplitude was observed in September 2024, mirroring the patterns typically seen during summer.

Wind-Induced Near-Inertial Oscillations

The Slab Model, initially introduced by Pollard and Millard in 1970, has been extensively utilized to simulate NIOs in the near-surface ocean. To explore the potential generation of inertial oscillations by local winds in the shallow shelf region off Concepción, mixed-layer velocities were simulated using the following equations:

$$\frac{\partial u}{\partial t} - fv = \frac{\tau_x}{\rho H} - ru$$

$$\frac{\partial v}{\partial t} + fu = \frac{\tau_y}{\rho H} - rv$$

Equations 01: The damped slab model equations for horizontal velocities, as described by Pollard and Millard (1970), are given by (u, v) (Equation 1.1), where (u) and (v) represent the zonal and meridional mixed layer velocities, respectively. In these equations, (τ_x) and (τ_y) are the zonal and meridional components of wind stress, (H) is the mixed layer depth, (ρ) is the water density, and (r) is the damping rate (decay) of NIOs.

From Equation 01, u and v represent the horizontal zonal and meridional velocities of the near-surface ocean, τ_x and τ_y represent the zonal and meridional components of the wind stress, H represents the mixed layer depth, f represents the local Coriolis parameter, (ρ) represents the density of seawater, and r represents a damping rate for NIOs decay. Since the rotary spectra and rotary wavelet transform analysis of the near-surface current velocities did not reveal a significant shift in the local Inertial frequency, we simplify the equations to a linear slab model, as described by Wang et al. (2023). This simplified model predicts the NIOs given initial velocity, mixed layer depth, wind stress, and damping rate. The Slab model is an unstratified model, meaning that the only natural frequency considered is the inertial frequency (f). To account for dispersion effects and the decay of NIOs in the surface mixed layer, a linear damping term ($-r$) is incorporated. The decay factor is determined as described by D'Asaro (1989).

The mixed layer depth (H) was determined using a method outlined by Holte and Talley (2009), using Argo and CTD profiles of temperature and salinity near the mooring location (L1). Each profile was used to compute the mixed layer depth, which was then

temporally interpolated to match the resolution of the hourly wind stress time series. The wind stress components were calculated using the following equations:

$$\tau_x = \rho_a C_d (U_{10}^2 + V_{10}^2)^{1/2} U_{10}, \quad (2.1)$$

$$\tau_y = \rho_a C_d (U_{10}^2 + V_{10}^2)^{1/2} V_{10}, \quad (2.2)$$

Equation 2: The zonal and meridional component of the wind stress are represented in equations 2.1 and 2.2. Where $\rho_a = 1.22 \text{K g/m}^{-3}$ is the density of the air, C_d denote the drag coefficient of the air according to Large and Pond (1981), the zonal and meridional wind velocity (u, v) are represented by the wind from the Hualpen weather station, located near te mooring L1.

Where $\rho_a = 1.22 \text{K g/m}^{-3}$ is the density of air. C_d denotes the drag coefficient calculated using the method developed by Large and Pond (1981). U_{10} and V_{10} represent the zonal and meridional wind speeds at 10 m above the sea level. The slab model was forced with hourly winds from the Hualpén and Carriel-Sur weather stations (indicated by CS and H on the figure 3), and reanalysis winds from E RA5. Weather station data for January 2005 was downloaded from the [DGAC](#) website. ERA5 hourly wind data, a reanalysis product combining model data with observations from around the world, was downloaded from the [Copernicus](#) website. Additionally, wind data from the onboard weather station of the coastal buoy [POSAR](#) located near L1 was used to evaluate the wind properties over the shallow ocean near the coast. The slab model performed best when forced with in-situ winds from weather stations. In contrast, the ERA5 reanalysis winds did not accurately represent the diurnal weakening of wind observed at weather stations during the summer season, thus affecting the model's wind-induced circulation results. Similarly, the empiric modes of decomposition and energy distribution of ERA5 winds differed significantly from the wind data collected at coastal weather stations.

Satellite SST

The surface thermal structure over the continental shelf of Concepción during January 2005 is described using a daily composite of sea surface temperature (SST) generated from multiple sensors. This composite was created by combining Level 2 polar-orbiting infrared sensor data from multiple satellites, including Aqua MODIS, Terra MODIS, AVHRR Suomi-NPP, and AVHRR NOAA-20. By integrating up to four satellite measurements per day, the temporal and spatial resolution of the data were significantly enhanced, thereby ensuring the accuracy of the satellite-derived information, spacially in areas near the coast. The Level 2 remote sensing data were extracted from the NASA Ocean Color website and processed using SeaDAS, WimSoft, and Python. A total of 126 images were processed for January 2005 using the Windows Image Manager software, along with its accompanying automation module, WAM, which was developed by Dr. Mati Kahru of WimSoft.

Ocean models and Lagrangian circulation.

The HYbrid Coordinate Ocean Model (HYCOM) serves as an invaluable tool for evaluating NIOs in the upper layers of the ocean (Raja et al. 2022). By integrating high-resolution data with a sophisticated three-dimensional representation of ocean dynamics, HYCOM can accurately simulate the interactions between wind forcing and ocean response, particularly in capturing the generation, propagation, and dissipation of NIOs in coastal areas (Chassignet et al. 2007). This model uses a hybrid coordinate system that dynamically adjusts to better represent both the well-mixed surface layers and the stratified deeper waters, making it especially effective for studying how wind energy at the surface translates into inertial currents. Recently, a comparison of the most widely

used numerical models in oceanography (ROMS, MITgcm, MIKE, and HYCOM) indicates that over the Gulf of Mexico, HYCOM captures the dominant circulation patterns, including cyclonic and anticyclonic motions across a wide range of frequencies. This suggests that HYCOM produces results similar to those of numerical models specifically generated for the study area.

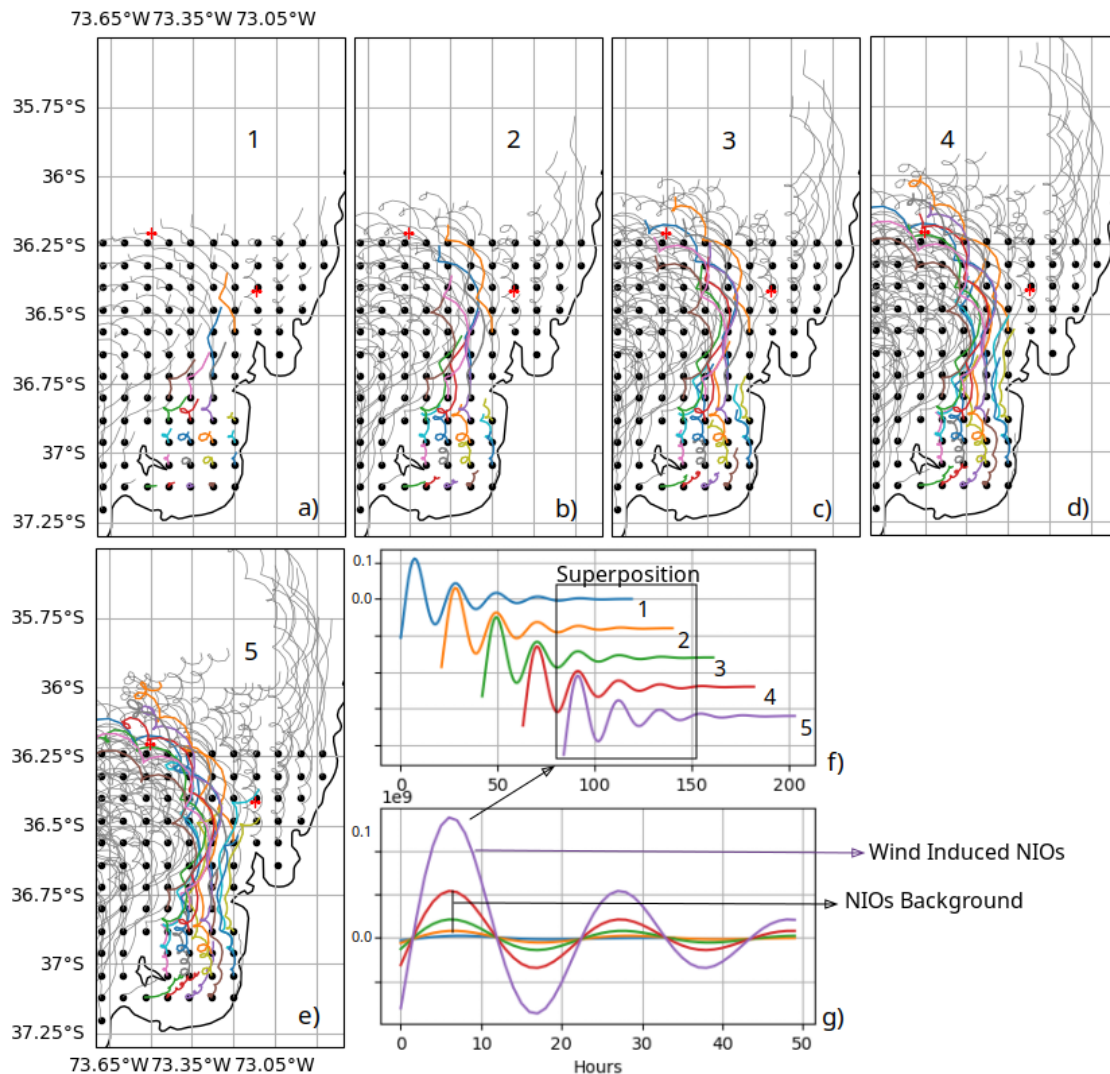


Figure 04: Near-surface simulated diurnal Lagrangian circulation over 5 days is represented in panels a, b, c, d, and e, with the red cross indicating the position of location L1. Panels (f) and (g) illustrate the interaction-superposition between locally wind-induced NIOs and the decay velocity of traveling NIOs to the location L1.

The movement of particles over the Concepción continental shelf is evaluated using the Python-based Ocean Parcels model (Delandmeter and Sebille 2019), which simulates Lagrangian circulation with a particular focus on NIOs. Ocean Parcels is a three-dimensional Lagrangian particle tracking framework that is compatible with outputs from various Ocean General Circulation Models (OGCMs). This model can track both passive and active particles, such as water, plankton, plastics, and fish, providing an efficient method to assess the impact of NIOs on particle dispersion. In this study, the Parcels model was driven by near-surface horizontal current velocities provided by the HYCOM data. The Lagrangian circulation over the continental shelf for a 5-day period in January 2005 are depicted in panels a, b, c, d, and e.

Results

General observation of Near-Inertial Oscillations from horizontal currents.

NIOs are the dominant and only significant frequency peak observed in the negative rotary spectra of the first baroclinic mode of the horizontal velocities between 5 and 90 meters depth. This mode accounts for 63% of the total horizontal current variance, emphasizing the dominance of NIOs throughout the entire water column during January 2005. Horizontal current velocity measurements in the upper ocean demonstrate that NIOs can be identified from the negative rotary spectra starting at a depth of 5 meters (refer to panel a, Fig. 4). At 4 meters depth, the current predominantly follows the wind direction, while at 5 meters depth, it begins to rotate counterclockwise in response to an initial pulse of energy and the Coriolis force. The near-surface ocean above 5 meters depth does not display any significant energy peaks at any frequency in the rotary spectra, exhibiting only background energy that decays from geostrophic to buoyancy frequencies.

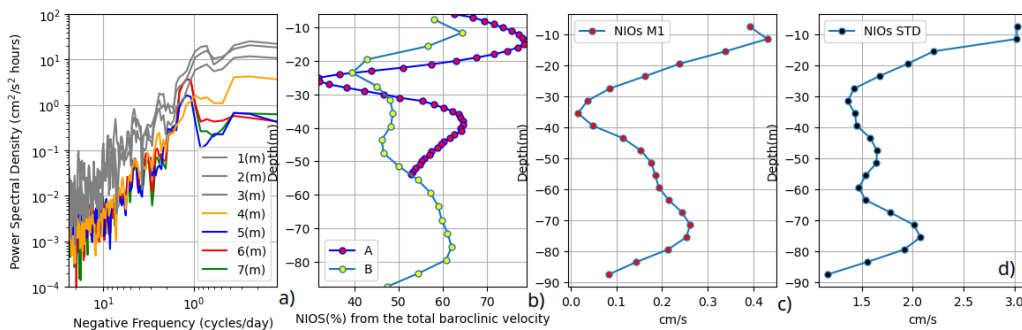


Figure 04 : Panel (a) shows the negative rotary spectra for the upper 7 meters of the ocean during 10 days of measurements. Panel (b) presents the percentage of NIOs as derived from the baroclinic average velocity throughout the water column. The data are based on two distinct measurement sets: Line A: Displays the 10-day average percentage of NIOs, captured by a downward-facing Acoustic Doppler Current Profiler (ADCP). Line B: Shows the 27-day average percentage of NIOs, recorded by a bottom-mounted ADCP. Panel (c): Here, the first mode of variability in the NIOs velocity is depicted. Panel (d): Represents the standard deviations of the NIOs velocity over a 27-day measurement period.

The rotary spectra of the total current (barotropic + baroclinic velocities) reveal a dominance of anti-cyclonic motions over the internal rotary wave band for all depths, with inertial and diurnal frequencies the strongest anticyclonic motions. Negative rotary spectral analysis conducted over 5-day intervals during a 25-day measurement period revealed a dominant presence of the inertial frequency. In contrast, the diurnal frequency exhibited strong synoptic fluctuations. The near-inertial peak of energy becomes broader when there is a contribution from the diurnal rotary frequencies. Panel (b) of Figure 2 depicts the percentage of NIOs derived from the average baroclinic velocity, measured over 10 days at high vertical resolution (1 meter, A), and over 27 days at lower vertical resolution (4 meters, B). During the month, more than 60% of the baroclinic velocities are dominated by NIOs in the upper ocean and near the bottom, with the weakest dominance observed at approximately 20 meters depth, corresponding to the base of the thermocline. The shortest time series (A) exhibits a similar structure in the upper ocean, reaching nearly 80% NIOs dominance and weakening to around 30% at approximately 25 meters depth. In terms of velocity, the strongest near-inertial current can reach up to 8 cm/s, with an average of 3 cm/s, primarily located in the upper ocean. The NIOs extracted from the baroclinic velocities exhibit anticyclonic ellipses, with maximum major and minor axes of 2.5 kilometers in the upper ocean, above the thermocline. The

first mode of variability via PCA of the NIOs velocity explains 53% of the total variance and is represented in panel (c) of Figure 4. The first mode shows a decay in the NIOs velocity from the near-surface ocean to 35 meters depth, reaching velocities of 0.4 m/s in the near-surface; an intensification near 70 meters depth is detected by the same mode with velocities of 0.25 cm/s. Similar to the first mode, the standard deviation shows the stronger fluctuation of the NIOs velocity in the upper ocean above 30 meters depth. The current trajectory indicate the downward radiation of the counterclockwise rotary horizontal velocity during specific time windows. However, for the most part, the rotary velocity remains confined to the upper ocean. Contrary to the horizontal currents, where NIOs are detected at all depths, the vertical current calculated from the horizontal velocities shows weaker near-inertial fluctuations only near the 20-meter depth. Near-surface drifters from the NOAA Global Drifter Program measure the Lagrangian trajectories of the upper 15 meters of the ocean globally. Strong rotary trajectories with strong near-inertial frequencies were detected in drifters near the shelf break close to the location L1, the NIOs velocity from drifter represent 42% of the total current velocity variability.

NIOs modified by sub-inertial velocity

Panel (a) of Figure 5 represents the progressive diagram of the NIOs rotary trajectory modified by the filtered sub-inertial velocity, with the velocity in cm/s represented in colors. It is clearly observed from the panel that weak sub-inertial velocity is associated with strong rotary trajectories. The surface summer NIOs trajectory is simulated analytically using a diurnal wind amplitude of 8 m/s and a shallower mixed layer depth to evaluate the impact of increasing sub-inertial velocities on the rotary trajectory of NIOs. Panel (c) of Figure 5 illustrates multiple NIO trajectories; the trajectory at the top, labeled with the number 1, shows the NIO trajectory during 10 inertial cycles modified by a weak sub-inertial horizontal velocity of 0.05 m/s. In the absence of significant sub-inertial velocity, pure inertial oscillations would continue to rotate in the same location until their complete decay and dissipation. However, as represented, increasing the sub-inertial velocity (2-9) completely deforms the rotary properties of NIOs, causing them to lose their intrinsic retention properties. Originally, a NIO completing one rotational cycle in approximately 20 hours can retain almost five times the displacement of the current when forced by a sub-inertial velocity of 0.08 m/s. This suggests that even under optimal conditions for local NIO generation at the ocean surface, relatively weak sub-inertial currents are essential for maintaining their rotary trajectory. Furthermore, our basic simulation model based on the slab model suggests an accelerated decay rate of NIOs in the presence of stronger sub-inertial currents. For instance, NIOs initiated by an 8 m/s wind force with sub-inertial velocities between 0.03-0.04 m/s exhibit a lifespan of approximately 5 days. However, this duration significantly reduces to 1-2 days with an increase in sub-inertial velocity to 0.08 m/s.

Near the surface, the rotary trajectory of NIOs is significantly influenced by sub-inertial velocities induced by wind, decaying within the first 20-40 meters of depth. The strongest NIOs are observed during periods of weak sub-inertial currents, with velocities less than 3 cm/s. The downward radiation of the NIOs rotary trajectory is evident from panel (a) during January 3-6, where weak sub-inertial velocities affect the entire water column. The downward NIOs radiation event correlates with an intensification of the cold upwelling thermal front (panel c), reducing the stratification and allowing the downward radiation of the rotary velocity. Prior to the event, the upwelling cold front was weaker (panel b), and the sub-inertial velocity was stronger in the upper ocean above 70 meters depth.

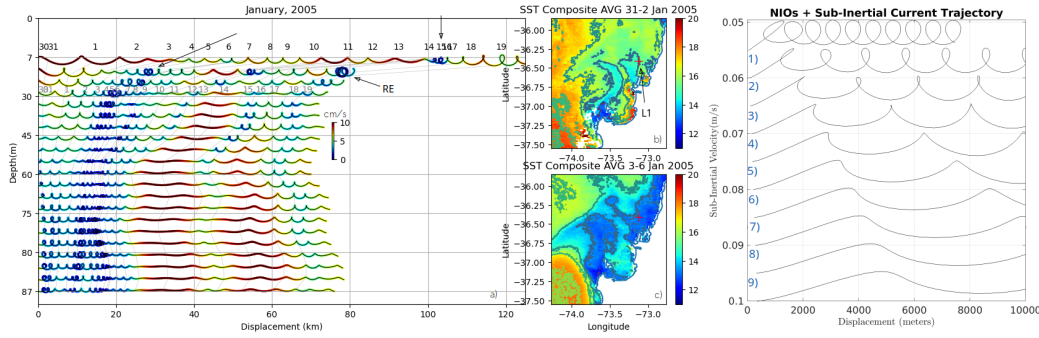


Figure 05: Panel (a): Illustrates the trajectory of NIOs modified by the filtered sub-inertial circulation during January 2005. The velocity of the sub-inertial current is denoted by color, with units in cm/s. Panels (b) and (c): Display the composite average of Sea Surface Temperature (SST) across two distinct intervals: Panel (b) covers the period from December 31, 2004, to January 2, 2005, while Panel (c) extends from January 3 to January 6, 2005. A red cross in both panels indicates the location of point L1. Panel (d): Depicts the simulated interaction of Near-Inertial trajectories with incrementally increasing sub-inertial velocities during the summer season.

During a period of strong sub-inertial horizontal velocities, reaching nearly 10 cm/s between January 13th and 18th, the weakest NIOs were observed. This strong current velocity perturbed the water column from the bottom up to approximately 20 meters depth, with a dominant southward direction near the bottom. This southward current velocity correlated with a strong synoptic cold thermal front, detected by both the SST composite at the L1 location and temperature profiles, which persisted for four days. These intense sub-inertial velocity events may represent a baroclinic response to the strong upwelling circulation. Conversely, a near-surface weakening of the sub-inertial current, accompanied by strong NIOs, was detected during a wind relaxation event. Unlike previous events, the rotary trajectory of these NIOs was pronounced only in the upper ocean, above 20 meters.

Surface NIOs vertical distribution controled by thermal structure.

The vertical distribution of NIOs at location L1, characterized by their downward radiation, is significantly influenced by the synoptic thermal structure of the water column. Figure 6b illustrates the velocities of the NIOs. In this figure, the orange line represents the average SST within a 0.15-degree radius around location L1, while the black line indicates the 12 °C thermocline derived from the thermistor chain installed at L1. SST data for the month of January 2005 reveal strong variability in the upwelling thermal front and coastal temperatures, the thermal synoptic fluctuations is mostly induced by upwelling and relaxation events over the study area. Panel (a) represents the diurnal average temperature profile from January 16 to 26, indicating nearly homogeneous vertical profiles with weak thermal stratification on January 16, transitioning to a strong thermocline and enhanced thermal stratification by January 24.

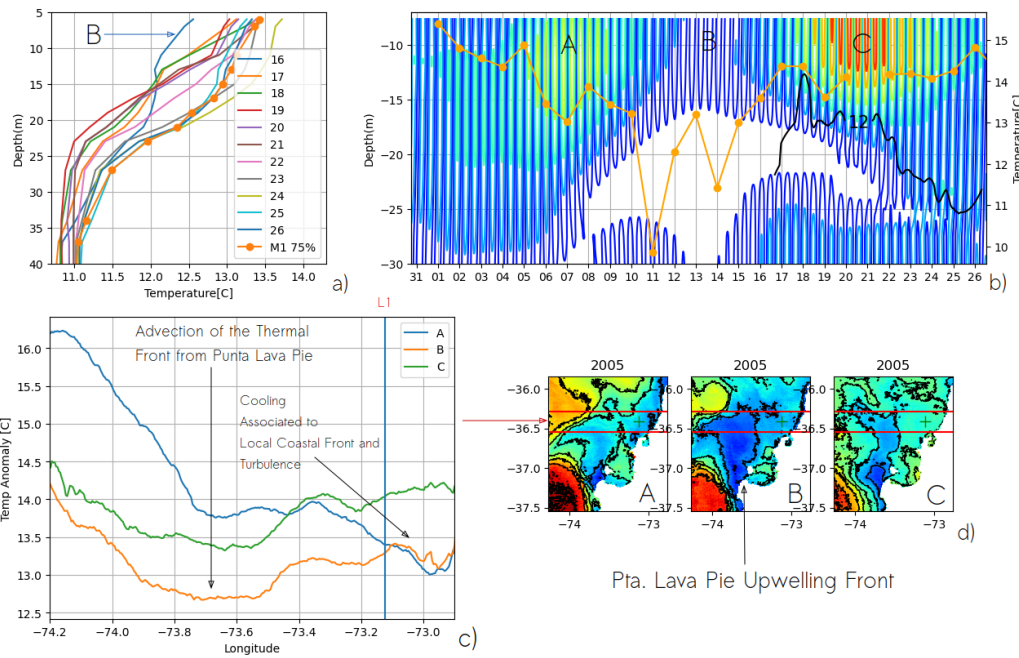


Figure 6: Panel (a): Displays the diurnal average temperature of the water column from January 16th to 26th. The first mode of the temperature is highlighted in orange. Panel (b): Shows Near-Inertial Oscillations (NIO) velocity between 7 and 30 meters depth. The orange line represents the average sea surface temperature (SST) within a 0.15-degree radius around location L1 (as defined in Figure 6). The black line marks the 12°C thermocline, derived from the thermistor chain installed at location L1. Panel (c): Presents the longitudinal thermal average from SST at location L1 during three specific times (A, B, and C). Panel (d): Depicts the sea surface temperature average during times A, B, and C, as indicated in panel (b).

The vertical distribution of NIOs in the upper ocean above 30 meters depth exhibits a strong correlation with the SST at location L1. The weakest NIOs (B) were detected during the coldest SST ($<13.5^{\circ}\text{C}$) times at the coastal location L1, which coincided with the advection of a cold front from Pta-Lavapie, as depicted in panel c (orange line), and panel d (B). An examination of the SST longitudinal section (area between red lines over panel d) at the latitude near L1 reveals that the L1 location experiences local thermal fluctuations between the L1 position and the coast, as well as thermal perturbations caused by the north-ward advection of the cold thermal front from Punta Lavapie (panel c). In contrast, strong NIOs (Panel b, events A–C) were detected during warmer SST ($\sim 14^{\circ}\text{C}$) and strongest thermal stratification associated with a relaxation of the upwelling, in which NIOs can reach depths of up to 30 meters. NIOs events A and C, as shown in Panels b, c, and d, show a different thermal distribution between offshore and the L1 coastal location, where the strongest NIOs are related to warming temperatures (green line in panel c). This occurs even when offshore SST is colder, indicating times when the coastal spatial thermal distribution differs from offshore during strong thermal stratification events associated with relaxation of upwelling. During event B, there appears to be synchronization between the advection of the upwelling thermal cold front from Punta Lavapie and coastal processes at location L1, resulting in a significant reduction in the thermal stratification of the water column. Clearly, the intensity of NIOs in the upper ocean is strongly related to the thermal stratification of the coastal ocean.

The first mode of the temperature profiles between January 16 and 26 reveals a strong thermocline near 20 meters depth that decays near 30 meters depth, accounting for 75% of the total temperature variance (panel a, Figure 6). This mode represents a thermally stratified ocean, where NIO velocities can reach depths of approximately 25-30 meters. During January 2005, the input of freshwater from local rivers and precipitation to the coastal location did not significantly affect the thermal stratification at location L1. However, diurnal Integrated Water Vapor (IWV) data for January 2005 show atmospheric rivers near the central south of Chile, bringing a substantial amount of precipitation that

could potentially alter thermal stratification in the upper ocean affecting NIOs vertical radiation. The atmospheric river did not reach the mooring location, instead precipitating offshore.

NIOs Decay

The velocity of NIOs in the coastal ocean exhibits significant decay with depth. From the near-surface down to approximately 25 meters, the average NIO velocity decreases from 0.4 cm/s to 0.1 cm/s (± 0.05 cm/s, as shown in Panel A). The first vertical mode of NIO velocity, which accounts for 53% of the total variance, shows this decay extending to nearly 35 meters below the surface (Panel A). In the upper ocean, specifically above a depth of 40 meters, the NIO velocity generally decays or dissipates to a minimum (indicated by blue color in Panel B, Figure 7). However, beyond this depth (Panel C, Figure 7), the velocity begins to increase, suggesting an influx of external near-inertial energy, possibly from advected NIOs or locally generated near-inertial motions. The decay profile of diurnal NIOs is depicted in Panels B and C of Figure 7, between depths of 10-40 meters and 40-90 meters, respectively. The color gradient in these panels represents the NIO velocity.

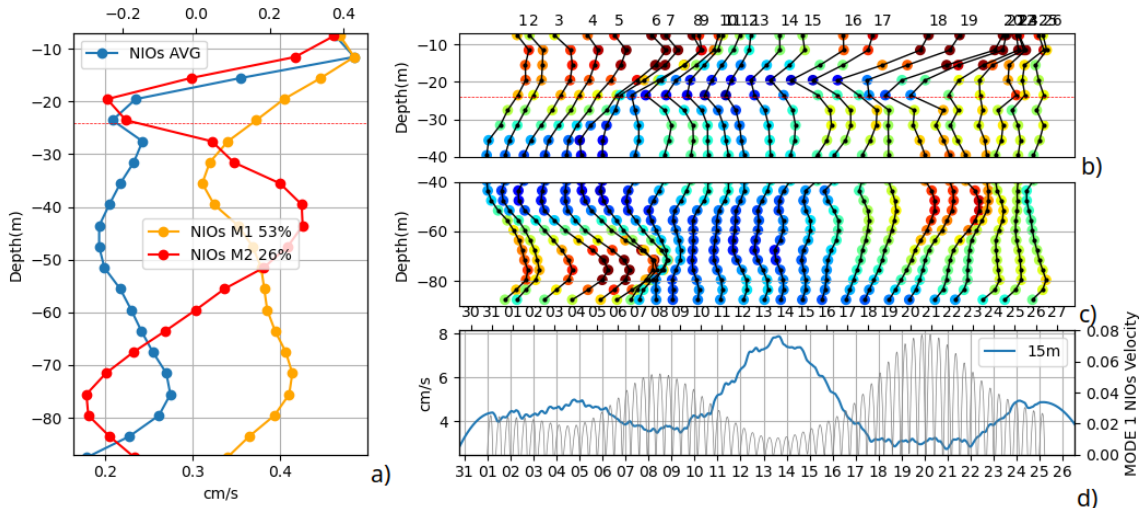


Figure 7: Panel (a) presents the average velocity of NIOs during January 2005, along with the first and second vertical modes of the NIO velocity profile. Panel (b) illustrates the diurnal average structure of the NIO velocity between January 1 and 26, with colors indicating the magnitude of the NIO velocity. Panel (c) shows the baroclinic velocity at a depth of 15 meters, as well as the temporal first Empirical Orthogonal Function (EOF) mode of the NIO velocity.

The vertical decay of NIOs in the upper ocean to their minimum velocity shows fluctuations, particularly between depths of 20 to 40 meters, where approximately 70% of NIO energy is dissipated. From January 21 to 25, there is no detectable minimum velocity in the upper ocean, suggesting either a continuous transfer of NIO velocity from the near-surface to deeper layers or the influence of an external source of NIOs not induced by local winds. The depth at which NIO velocity reaches its minimum value exhibits synoptic variability, largely influenced by changes in coastal stratification due to upwelling and relaxation events that control the mixed layer depth. Deeper decay is correlated with the relaxation phases of upwelling events and the presence of deeper, stronger thermoclines, as observed from January 1 to 12. Conversely, during intense upwelling periods, identified by colder SST from satellite data, the vertical decay to minimum velocity occurs at shallower depths, around 20 meters. Below 40 meters, there is a period of continuous NIO decay from the upper ocean to the bottom, interspersed with periods of intensification at mid-depths or near the bottom, which eventually dissipate. Throughout the water column below 40 meters, NIO velocities can reach values

similar to those observed near the surface during upwelling relaxation events. However, the weakest velocities are observed during periods of strong upwelling currents that last for three or more days.

Horizontal velocity measurements also play a crucial role in determining the decay depth of NIOs in the upper ocean. Strong sub-inertial velocities detected during upwelling events significantly alter the rotary properties of NIOs, accelerating both their vertical and horizontal decay. Panel D, figure 7 shows the first mode of horizontal NIO velocity alongside sub-inertial velocity at a depth of 15 meters, illustrating how near-surface NIO velocity experiences a shallower decay during periods of strong sub-inertial currents.

NIOs Shear and mixing

The shear of turbulence in the upper ocean is evaluated with high vertical resolution horizontal current measurements (1-meter intervals) using the following equation:

$$S = \sqrt{(\frac{\partial u}{\partial z})^2 + (\frac{\partial v}{\partial z})^2}$$
. The equation represents the shear production of turbulence,

where (S) denotes the magnitude of shear based on the vertical gradients of the horizontal velocity components u and v in cm/s. Figure 8, panel (a) depicts the shear of turbulence between January 15 and 25, showing intense shear in the upper 30 meters of the ocean. This strong shear is observed above the thermocline and is associated with depths where the Brunt-Väisälä frequency indicates a breakdown in the stability of the water column (panel b). In contrast, stable water columns exhibit weak shear. The

Richardson number, calculated using the following equation $Ri = \frac{N^2}{(du/dz)^2}$ where (N) is

the Brunt-Väisälä frequency and ($\frac{du}{dz}$) is the vertical shear of horizontal velocity, indicate a stratified water column at depths with strong horizontal shear. This indicates potential vertical mixing and an unstable flow at depths of strong shear. Over the 10-days period of 1-meter vertical resolution current measurements, over 90% of the horizontal shear of turbulence is concentrated in the baroclinic mode of the current (Figure 8c). Within this baroclinic mode, approximately 65% of the shear is associated with NIOs above the thermocline near ~20 meters depth, as indicated by the first mode of the temperature (Figure 8, panel d). The vertical average profiles of horizontal shear from NIOs, baroclinic, and total velocities are shown in Figure 8, panel c. The strong shear of turbulence detected between January 19-22, correlates with a along-shore wind relaxation event and strong rotary trajectories of NIOs, which travel downward to the base of the thermocline. The square in Panel (a) represents the horizontal shear of turbulence during the transition from strong upwelling circulation to relaxation, as identified by coastal Sea Surface Temperature (SST).

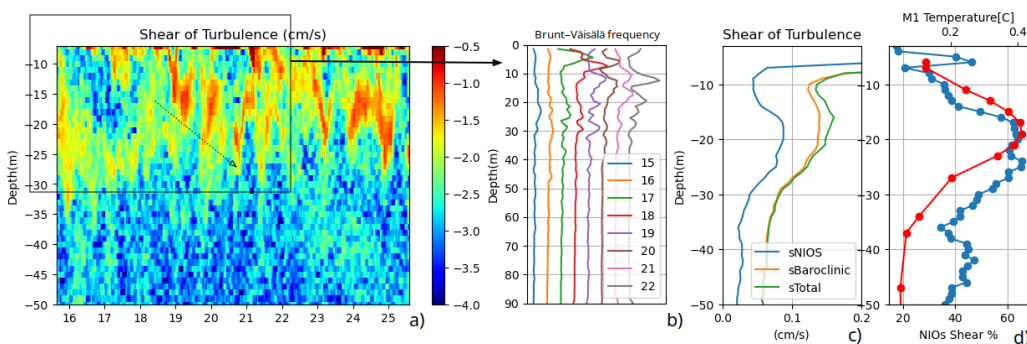


Figure 8: Panel (a) represents the shear of turbulence between January 15 and 26. Panel (b) shows the Brunt-Väisälä frequency between January 15 and 22, based on the diurnal average of temperature and salinity profiles at location L1. Panel (c) depicts the shear of turbulence for the NIOs, baroclinic, and total current velocity. Panel (d) shows the percentage of shear velocity associated with NIOs (blue line) and the first vertical mode of temperature (red line).

A lower vertical resolution of horizontal currents (4 meters) was also used to calculate the horizontal shear of turbulence along the water column. It is acknowledged that the accuracy of the shear measurements is limited due to the lower vertical resolution. Despite this limitation, a similar pattern in the upper ocean was found in relation to the high vertical resolution time series. Throughout the month, most of the shear is located in the upper 30 meters of the water column, with a significant amount of turbulence near the bottom, associated with strong rotary current velocities that last for 6 days. The low-frequency shear of turbulence shows significant spans of shear in the upper ocean, particularly during times of strong cold fronts at location L1. Over an unstratified ocean, the shear of turbulence is weaker than during a stratified water column; however, it still indicates a resultant interaction between surface Near-Inertial Oscillations (NIOs) and coastal thermal fronts that could lead to shear. Strong thermal fronts were detected through sea surface temperature observations near location L1 (Figure 1). The first cold front (F1, figure 1) is associated with the advection of a cold plume originating from Punta Lavapié, which extends towards the vicinity of L1, while the second front (F2, figure 1) is associated with coastal boundary upwelling and local wind-induced turbulence.

Significant shear of turbulence was also detected near the ocean bottom. This shear correlates with strong NIOs that have a current trajectory directed towards the coast. The path of these currents suggests that the traveling NIOs might have been generated near the bottom, likely due to interaction with the coastal topography or bottom friction. As shown in Panel (d) of Figure 8, the variability in horizontal shear of turbulence closely follows the first mode of the vertical temperature structure, indicating a strong relationship between the thermal structure and horizontal shear at location L1.

NIOs and Near Inertial Internal waves

A wind-relaxation event, identified using the method described by Melton, Washburn, and Gotschalk (2009), coincided with a significant accumulation of NIOs that radiate downwards (Fig. 5, Panel a) between January 17th and 19th. Panels (a) and (b) of Figure 9 illustrate the zonal (u) and meridional (v) components of the NIOs velocities, with the red arrow indicating the radiate direction of NIOs. The velocity of the NIOs transferred from near-surface reaches depths of nearly 20 meters. The interaction between the downward radiate NIOs and the thermally stratified layers of the ocean led to the generation of the secondary manifestation of inertial motions: near-inertial internal waves (NIWs). The NIWs were observed in the near-inertial filtered temperature data, as shown in Panel (c), with thermal fluctuation of 0.5-1 celcius degrees. The longitudinal diurnal average of SST near L1 (Panel e) reflects the thermal stratification, with weaker stratification corresponding to colder temperatures around 13.5°C and stronger stratification corresponding to temperatures around 15°C .

As the near-inertial motions from the surface NIOs penetrated deeper, the NIWs followed the thermocline structure to depths below the base of the thermocline (Panel c), reaching approximately 35 meters. Spectral analysis of the first mode of temperature data from the thermistor chain at L1 revealed a dominant peak of energy at the near-inertial frequency. This first mode explains 56% of the variance in the temperature time series.

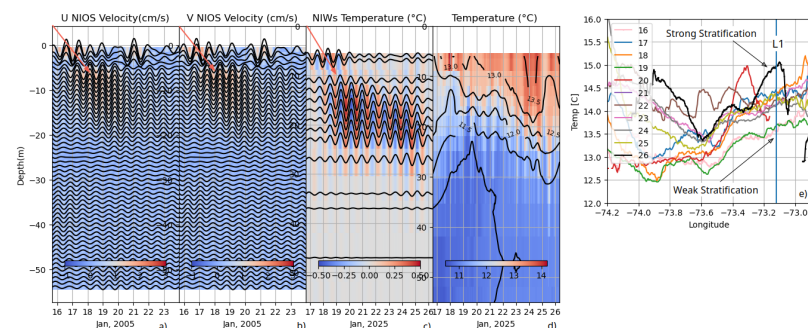


Figure 09: Panels (a) and (b): These panels illustrate the near-inertial horizontal current velocities (in cm/s) for the along-shore and cross-shore directions, respectively. Black lines overlaying the current velocity trace the intensity of these inertial motions, highlighting fluctuations over time. Panel (c): This panel shows the temperature profile of the water column, filtered to highlight variations within the near-inertial band. The data suggest that the water column is significantly perturbed by near-inertial internal waves, which can influence mixing and energy transfer within the ocean. Panel (d): Here, the temperature of the water column is presented over depth. The black line delineates pronounced thermoclines, indicating layers where temperature changes rapidly with depth. This panel provides context for the thermal structure and near-inertial internal oscillation (NIO) velocities of the ocean during the observation period.

The shorter vertical temperature time series indicate that Near-Inertial Waves (NIWs) are trapped by the thermocline, suggesting an area with strong vertical fluctuations in ocean properties, where there is a concentration of near-inertial energy that could lead to mixing. The diurnal section of longitudinal sea surface temperature (SST) indicates a strong relationship between strong NIWs and warmer temperatures, serving as a proxy for a stratified water column (panel e).

Local winds and wind induced NIOs

Coastal surface wind data, collected from satellite observations and weather stations in January 2005, revealed a predominantly upwelling-favorable wind regime, interspersed with brief periods of wind relaxation and downwelling-favorable events. Analysis of wind velocity data from weather stations indicated that the diurnal frequency was the most dominant signal, particularly in the cross-shore wind component where it exhibited the strongest amplitude. Additionally, a synoptic signal with a periodicity of 4-5 days was evident in the wind spectrum, notably more pronounced in the along-shore wind component. The diurnal velocity of the cross-shore wind intensified as it approached the coast, in contrast to the along-shore wind velocity, which decayed. Notably, only the negative (upwelling-favorable) along-shore winds maintained a consistent velocity across the continental shelf near the study area, showing no signs of either intensification or decay towards the coast. Previous research emphasizes the importance of intensified diurnal winds in the generation of NIOs. To investigate the relationship between the dominant diurnal wind frequency and the local sea breeze, which intensifies the cross-shore wind towards the coast, we calculated the Sea Breeze Index (SBI). The SBI, defined by the equation $SBI = \pm \frac{U^2}{\Delta T}$ (Atkison 1995; Frysinger, Lindner, and Brueske 2003), depicts the relationship between synoptic wind and land-sea temperature differences, crucial for sea-breeze formation. From figure 10 panel (a), the positive y-axis represents the squared offshore cross-coast component of the synoptic wind, while the positive x-axis represents the temperature difference between air over land and coastal sea surface temperatures. The dashed, angled line represents the critical sea-breeze index value. The area below this index line and above the x-axis indicates the regime considered conducive to sea-breeze cell formation. Other areas on the plot represent different regimes, as indicated in the figure.

From the SBE equation, U represents the cross-shore component of the synoptic wind, and ΔT represents the temperature difference between the SST at location L1 and the overland air temperature measured at the CS weather station. To determine the cross-shore wind component, the wind velocity data from the CS weather station were rotated by -28 degrees to align with the coastal orientation as indicated by Frysinger, Lindner, and Brueske (2003). Subsequently, the cross-shore and along-shore wind components were extracted. The CS weather station provided air temperature measurements, and hourly SST data were obtained from ERA5 Reanalysis. This reanalysis data had previously demonstrated a strong correlation ($r = 0.87$) with satellite-derived SST measurements.

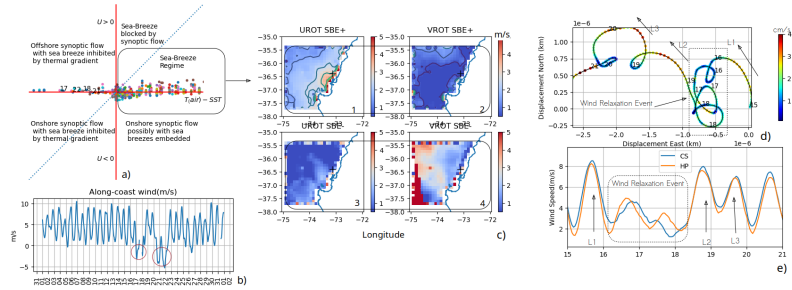


Figure 10. Panel (a) Sea-Breeze Index Plot: This panel depicts the relationship between synoptic wind and land-sea temperature differences, crucial for sea-breeze formation. The positive y-axis represents the squared offshore cross-coast component of the synoptic wind, while the positive x-axis represents the temperature difference between air over land and coastal sea surface temperatures. The dashed, angled line represents the critical sea-breeze index value. The area below this index line and above the x-axis indicates the regime considered conducive to sea-breeze cell formation. Other areas on the plot represent different regimes, as indicated in the figure. Panel (b) Cross-coast wind during January 2005. Panel c) Current Trajectory at a depth of 6 meters between January 15 and 21. Panel (d) Wind Speed: This panel presents the wind speed recorded by the Hualpen and Carriel Sur weather stations between January 15 and 21. Panel (e) This panel illustrates the anomaly in wind speed between the satellite's daily orbital revolutions, providing an approximation of the spatial and temporal anomaly of the diurnal wind speed amplitude.

The SBE index indicates that the sea breeze regime dominated during January 2005, with two events occurring between January 17–18 and January 21–22 (marked with red circles in panel b) during which the sea breeze was inhibited. During these periods, offshore synoptic flow suppressed the sea-breeze thermal gradient, and downwelling-favorable winds were detected. The sea-breeze index also shows that coastal SST responds to sea-breeze fluctuations, with near-coastal warm temperatures observed during the absence of sea-breeze induced diurnal winds.

Panel (d) illustrates the upper ocean current trajectories at a depth of 7 meters, with current velocities represented by color. Near the surface, the currents follow the wind direction toward the north, exhibiting diurnal acceleration and weakening patterns in response to the diurnal wind (indicated as L1, L2, and L3 in panels c and d). Below a depth of 5 meters, NIOs are detected (as revealed by the rotary spectra), the currents exhibit a dominant anticlockwise rotation indicative of inertial oscillations. During the summer, the diurnal winds are the primary source of momentum transferred from the lower atmosphere to the surface ocean. Wind velocity measurements from the HP and CS weather stations during January 15–20 are shown in panel (e), highlighting the diurnal wind amplitude (marked as L1, L2, and L3). A wind relaxation event occurred between January 16 and 18, during which the diurnal wind amplitude weakened by 55% compared to the climatological diurnal wind cycle for the month. The wind induces strong sub-inertial circulation along the current trajectories shown in panel (b), significantly modifying the rotary currents associated with NIOs, as discussed in previous sections. During the wind relaxation event (panel b) and the associated weakening of sub-inertial circulation (panel d), strong NIOs become evident, with three anticlockwise rotations observed following the initiation of a new inertial oscillation by the wind. These three rotary trajectories during the wind relaxation period demonstrate the horizontal decay rate of NIOs, which can persist for up to five days under weak sub-inertial circulation conditions.

Upper ocean observations indicate that the diurnal wind amplitude is the primary driver of NIOs over the upper ocean. Panel (c) shows the spatial intensification of the diurnal wind based on the average of QuickSCAT satellite scatterometer data from January 2005. The anomalies in wind speed between the satellite's daily orbital revolutions provide an approximation of the spatial intensity of the diurnal wind speed amplitude. Over the panel

(c), subpanel 1-2 indicate the u and v rotated satellite wind velocity anomaly during strong diurnal winds/sea-breeze detected by weather station and SBE index, contrary, sub-panel 3-4, indicate weaks diurnal winds anomaly (absence of sea breeze). Areas highlighted in red indicate the diurnal velocity intensification generated by the local sea-breeze cell, which intensifies the cross-shore wind. The momentum transferred from the lower atmosphere to the near-surface ocean, which induces circulation, is strongest near location L1, where the climatological diurnal wind amplitude is 4–5 m/s. Location L1 experiences strong diurnal wind amplitudes, which drive intense sub-inertial circulation and NIOs. Finally, the wind over the continental shelf of Concepcion, result from the interaction between the synoptic drop-off of the alongshore wind (panel a, figure 3) and the diurnal wind, which is primarily enhanced by the local sea breeze. The diurnal wind account for 65% of the variance in summer winds.

Simulated Wind induced NIOs

Wind stress data from the CS and HP weather stations were used to simulate mixed-layer velocities using the Slab unsteady wind model. The model was initialized with realistic conditions for mixed-layer depth, wind speeds, and air temperature. Initially, we simulated NIOs using a standard mixed-layer depth of 20 meters to understand the direct impact of winds over the mixed-layer velocities and NIO variability.

As illustrated in panel (a) of Figure 11, the simulated NIO velocities exhibit two distinct modes of variability during January 2005. The first mode, denoted by the black square labeled “A,” features a nearly constant NIOs amplitude with velocities averaging around 0.04 m/s. During this period, wind data from the CS weather station reveal a strong diurnal frequency in both the along-shore and cross-shore components, as indicated by spectral analysis (panels b and c). Weaker frequencies associated with synoptic variability are also detected for both wind components. In contrast, the second mode, illustrated by square B, shows NIOs velocities with a pronounced pattern of growth and decay over periods shorter than 5 days. The spectral analysis of the wind (panels b and c) driving this NIO variability reveals a strong synoptic (~5 days) frequency in the wind components, along with only a strong diurnal frequency in the cross-shore wind. Additionally, the along-shore wind exhibits a broader range of diurnal frequencies. The trajectory of the first mode (A) indicates a constant rotary current with a radius of approximately 1 kilometer. In contrast, the second mode (B) shows a sinoptic fluctuating rotary current, varying from a radius of 1 kilometer to a point where the rotary current is no longer detected.

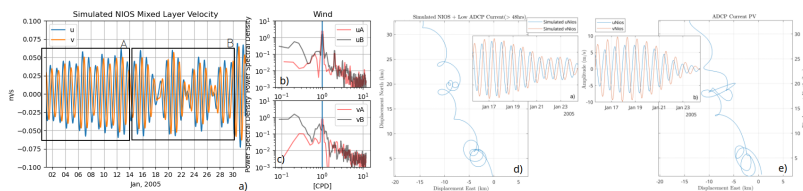


Figure 11: Panel (a) represents the simulated NIO velocities induced by the wind from the CS weather station. Panels (b) and (c) show the spectral analysis of the along-shore and cross-shore wind over squares A and B in panel (a). Panels (d) and (e) depict the trajectory of the simulated NIOs plus the low-frequency current, as well as the trajectory of the NIOs and low-frequency current measured by the mooring. Sub-panels indicate the simulated and measured NIOs.

A realistic mixed-layer depth was estimated using a combination of CTD profiles of temperature and salinity, thermistor chain data, and SST measurements. The CTD profiles captured a strong synoptic thermal change between upwelling and relaxation phases, which was also detected by SST from January 14 to 24 (Figure 6, panel b). The orange line in Figure 6b represents the diurnal average of SST around the L1 location, indicating thermal fluctuations during the month that alternate between relaxation and upwelling

events. The stratification at the L1 location is strongly influenced by temperature, showing a positive correlation between mixed-layer depth and surface temperature derived from satellite data. Shallower stratification over L1 is associated with the advection of the cold plume from Punta Lava as well as coastal mixing near L1. During periods of intense sea surface cooling (10°C) associated with upwelling-favorable winds, the mixed-layer depth, calculated from density profiles, was shallower, reaching approximately 5 meters. In contrast, warmer SST (14°C) corresponded to a deeper mixed-layer depth of around 25 meters and a stratified ocean. The mixed-layer depths calculated from CTD profiles were used to estimate the mixed-layer NIOs velocity from January 14 to 24. The simulated NIOs accurately reproduced the phase and most of the amplitude of the observed NIOs in the upper ocean. The weakest simulated NIOs velocities were detected during shallower mixed-layer depths, consistent with the observed NIOs velocities. Trajectories of sub-inertial velocities combined with simulated NIOs (panel d) and NIOs extracted from current velocities (panel e) at 5 meters depth are shown in panels (d) and (e) for January 15 to 25. These trajectories exhibit significant similarity, with a correlation of 0.71 between observed and simulated NIOs. The decay of the rotary trajectory of NIOs is strongly affected by the mixed-layer depth. During periods of deeper mixed-layer depth and stronger stratification, the decay in the upper ocean can last for up to 5 days. In contrast, during synoptic periods of shallower mixed-layer depth and weak stratification, the rotary velocity dissipates more quickly in the upper ocean.

Current trajectory and Simulated lagrangian circulation.

As represented in Section 3.2, the trajectory of NIOs is highly influenced by low-frequency currents. Under specific conditions, the NIOs' rotary decay trajectory under the influence of sub-inertial motions can be horizontally transported to L1 location from nearby areas. In this section, we evaluate the transport/advection of NIOs to the study area using in-situ and simulated velocities. A high correlation was found between the ADCP-observed trajectories in the upper ocean and simulated trajectories from the HYbrid Coordinate Ocean Model (HYCOM) simulated data ($R: 0.74$). Rotary spectral analysis indicates a similar dominance of frequencies between the observed and simulated data, with semidiurnal tides, diurnal frequencies, and NIOs being the most prominent. HYCOM's thermal structure also correlates with satellite and in situ data, detecting the thermal fluctuations between upwelling and relaxation events.

The dominant near-surface current direction at 8 meters depth is represented by arrows over location L1 in panel (a). The numbers within the arrows correspond to specific times shown in panel (b), which illustrates the trajectory of the water column at location L1 during January 2005, separated into sections of 100 hours. The trajectories in the upper ocean indicate a dominance of north, northeast, and east directions towards the coast. In contrast, deeper layers exhibit a dominant east and southeast direction towards the coast. Over these 100-hour segments, no predominant offshore (westward) current direction was observed. The trajectories suggest that most NIOs at L1 arise from the interaction between locally generated NIOs and those advected and decayed from offshore or southern coastal (near-bay) regions. In this context, near-surface decayed NIOs advected to location L1 are likely to be re-energized or intensified by the diurnal wind frequency, which in turn induces local NIOs. Current trajectories indicate that the strongest velocities in the water column are directed southward (SO4, SO3, Panel b). These velocities significantly modify NIOs, completely removing the inertial rotary circulation from the current trajectory. The strongest subsurface velocity correlates with the strong cold surface thermal front, suggesting a relationship between the coastal cold front induced by upwelling circulation and a southward response of the current velocity.

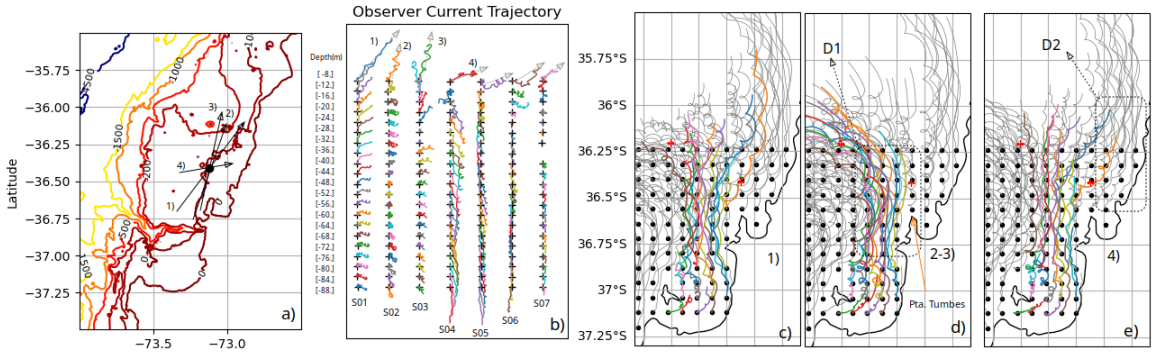


Figure 12: Panel (a) indicates the dominant near-surface direction of the current during specific times described in Panel (b). Panel (b) represents the current trajectory of the water column at location L1 during January 2005. Panels (c), (d), and (e) represent the simulated Lagrangian circulation in the near-surface ocean at a depth of 6 meters for the S01, S02, and S04 sections indicated in Panel (b).

The Lagrangian circulation of the simulated near-surface velocities (HYCOM, 8 meters depth) during periods S01, S02, and S04, as described in panel (b), is depicted in panels (c), (d), and (e). The dominant trajectory direction suggests a north and northeastward flow, which is consistent with the current trajectory detected by the ADCP (Acoustic Doppler Current Profiler). A significant acceleration of the current is observed over the areas denoted as D1 and D2, represented in panel (d-e) of Figure 12. This acceleration strongly alters the rotary trajectory of NIOs. South of the study area, the strongest NIOs are found in the Gulf of Arauco, where the sub-inertial current velocity is weak. These trajectories travel northward and accelerate as they pass under the D1 area, eventually reaching the northern side of the shelf near location L1 within approximately 3-4 days. Near the L1 coastal location (Punta Tumbes), near-surface NIOs may be generated locally along the coast and travel northward to the L1 location, indicating that these NIOs are locally generated with minimal contamination from nearby trajectories.

The current trajectory data from January 2005 suggest that the resulting NIOs at location L1 are a composite of wind-induced NIOs and a background of horizontal NIOs that have traveled to reach L1, as depicted in Figure 4. Figure 4 demonstrates that over location L1 during the first five days of simulated velocities in January 2005, locally generated NIOs interact with decayed NIOs that have traveled to this point. Here, the superposition of locally wind-induced inertial oscillations and the decayed NIOs represents the raw inertial velocity measured by the ADCP (Acoustic Doppler Current Profiler). The interaction between multiple inertial horizontal velocities can either intensify or weaken NIOs at this location. Within the study area, we identify two significant processes through which the interaction of multiple NIOs could modify their velocities: superposition and resonance.

Current velocity data from numerical models, in-situ measurements, and numerical experiments were utilized to assess the intensification of NIOs due to two key processes previously documented in similar coastal regions: superposition and resonance. Multiple analyses employing in-situ data were conducted to evaluate the growth and decay periods of the dominant frequencies within the time series, including diurnal, inertial, and tidal cycles. Additionally, numerical models were used to analyze the interaction of current trajectory and circulation patterns near location L1, indicating that NIOs are intensified by both superposition and resonance. **Superposition:** This process involves the summation of multiple signals with similar frequencies. Here, local NIOs interact with traveling or advected NIOs from nearby areas close to location L1. Superposition significantly increases the amplitude when the phases of these signals align closely. **Resonance:** The resonance in the study area was assessed by examining the dominant current frequency from the current spectrum. True resonance requires one frequency to match or be a harmonic of the local inertial frequency. However, in this case, the inertial, diurnal, and tidal frequencies do not share a simple harmonic relationship, leading to

what can be described as ‘pseudo-resonance’. This pseudo-resonance occurs when the phase alignment of cycles, like the 20-hour and 24-hour cycles, results in unusually high or low amplitudes due to constructive or destructive interference. Superposition emerges as the dominant mechanism for the interaction and intensification of NIOs at L1 location, particularly evident during January when the phases between local and traveling NIOs at L1 align in most of the water column velocity, leading to a strong intensification of horizontal inertial velocity. In contrast, pseudo-resonance exhibits both constructive and destructive responses between diurnal and inertial frequencies, enhancing or weakening NIOs, and inducing patterns of growth and decay, with variability near 5 days. Over the spectral analysis, the inertial frequency peak from resonance does not demonstrate the same level of intensification as observed with superposition.

Biological Consequences of NIOs

Vertical profiles of water column properties were measured using a CTD instrument (SBE 25) from January 14 to 22, 2005. Approximately 46 profiles were obtained at location L1, revealing two distinct scenarios in the water column properties, as clearly visualized from the diurnal SST in panel (a), Figure 11. From January 14 to 17, vertical and horizontal advection of denser subsurface waters (at about 14 meters depth) reached the surface at L1 location, as shown in panel (d). The mixed layer depth was shallow, around 5 meters. Oxygen concentrations in the upper ocean were below 5 milliliters per liter (mL/L). Fluorescence, an indirect measure of primary productivity, showed high values within the top 40 meters, suggesting significant local biological production. These characteristics indicate a strong upwelling event. Starting on January 17, a different scenario emerged. The density in the upper ocean decreased, indicating a reduction in subsurface water advection. The mixed layer deepened to approximately 20 meters, with stronger stratification. Oxygen levels rose above 5 mL/L, and fluorescence in the upper layers significantly decreased, pointing to a decline in surface primary productivity. Higher fluorescence values were observed near the base of the thermocline in the stratified water, as illustrated in panel (b). These changes suggest a relaxation of the upwelling circulation. Current trajectories in the upper ocean showed an offshore direction during the upwelling period and shifted to a southward direction during the wind relaxation phase.

A diurnal longitudinal section average of SST at the L1 location (panel e, figure 13) indicates that the northward advected offshore upwelling cold front from Punta Lava Pie does not lose intensity between the two scenarios detected by the CTD profiles. However, at L1, the SST clearly shows a warming trend from January 15 to 21. Satellite averages between the two scenarios reveal a slight intensification of the cold front at Punta Lava Pie, and significant northward advection of warm waters from the Gulf of Arauco during the relaxation event. These advected warm waters increase the temperatures at the L1 location, acting as a barrier that prevents the cold plume from Punta Lava Pie from reaching L1. During the CTD profile measurements times, panel (e) indicates that most surface temperature fluctuations are driven by local upwelling variations near the coast, rather than offshore advection.

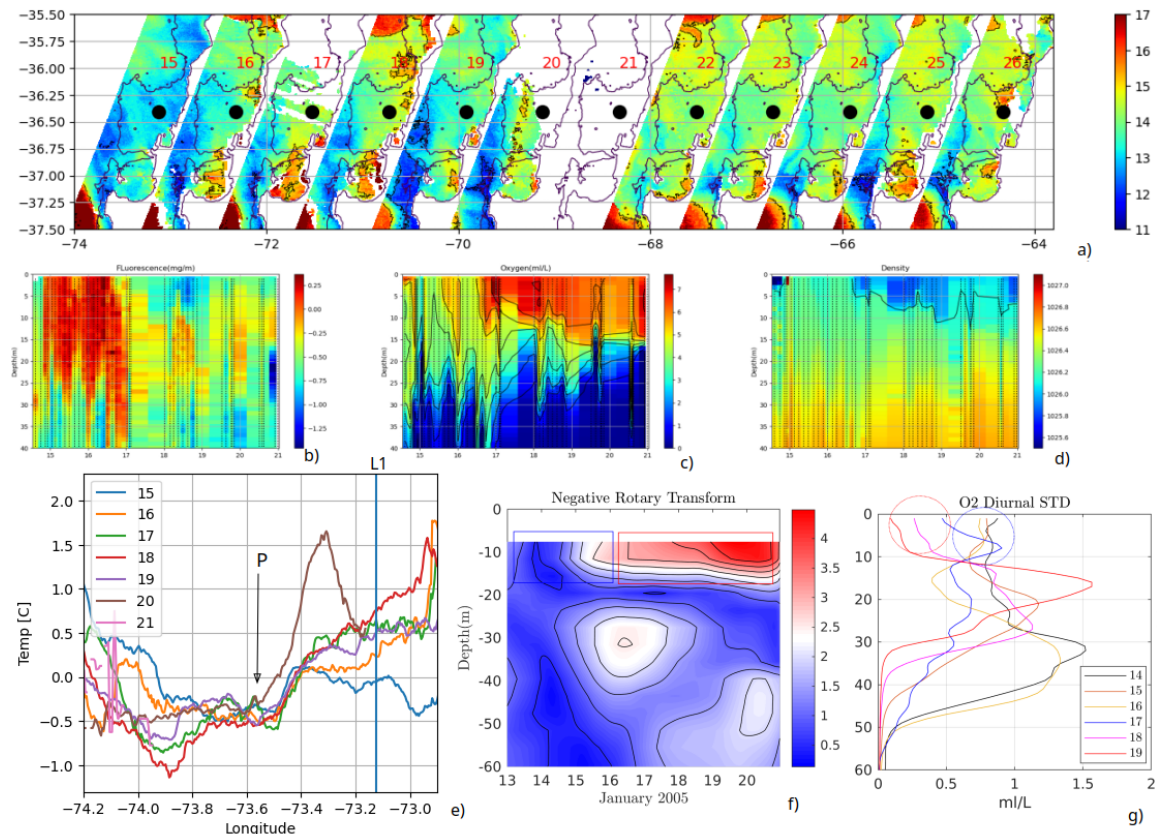


Figure 13. Panel (a) represents the diurnal Sea Surface Temperature (SST) from January 14 to 23, 2005, while panel (e) shows the averaged longitudinal section of diurnal SST centered at location L1. Hydrographic properties at location L1, recorded from January 15 to 21, 2005, are depicted in panels (e), (f), and (g) for fluorescence, oxygen, and density, respectively. Panel (f) also illustrates the negative rotary transform of the NIOs current velocity from January 13 to 21, with areas of strong NIOs highlighted in red. Additionally, panel (f) displays the standard deviation of diurnal oxygen profiles between January 14 and 23, 2005.

Between the coastal upwelling and relaxation at the L1 location, SST increases from a temperature anomaly of -0.5°C to $+1.5^{\circ}\text{C}$ near the coast. Associated with the warm advected waters, the mixed layer at L1 is deeper, the NIO velocities are intense, and the rotary trajectory of the current retains the coastal waters. Low-frequency variability of oxygen is mostly controlled by the sub-inertial circulation, but diurnal fluctuations of oxygen are primarily controlled by NIOs in the upper ocean. The standard deviation of the diurnal oxygen profiles is higher, near 1 mL/L during weak NIOs; conversely, the diurnal fluctuation of oxygen in the upper ocean between near-surface and 10 meters is significantly lower during strong NIOs (0.2 mL/L), indicating that the strong upper rotary velocity during the relaxation of upwelling homogenizes the surface water. The temperature above the thermocline ($\sim 15\text{-}20$ meters depth) shows higher variance with respect to the mean during intense near-inertial internal motions, which can reach up to 1.5°C difference during the day. Below the mixed layer depth, strong NIOs are correlated with higher fluctuation of the diurnal oxygen concentration between 20-40 meters depth.

Fluorescence during the relaxation events shows significant values below the upper ocean. During the relaxation, the increase in stratification generates a strong thermocline. The high values of fluorescence are located at the base of the thermocline, at depths where there is strong horizontal shear of turbulence. The depths of higher fluorescence during relaxation times correlate with strong inertial vertical fluctuations of temperature, inducing vertical fluctuations of the nutricline, playing an important role in nutrient uptake to depths near the thermocline.

Discussions

This study provides a comprehensive analysis of Near-Inertial Oscillations (NIOs) observed in the coastal ocean during January 2005 (summer). Our findings demonstrate that wind-induced NIOs are a dominant feature of the near-surface and subsurface current field, capable of vertically radiating to depths near the bottom, exerting significant influence on the dynamics and mixing processes within the study region. The observed dominance of NIOs in the baroclinic mode of the horizontal velocity field underscores their importance in shaping the vertical structure of the coastal ocean. The transition from wind-driven surface currents to NIOs at depths exceeding 5 meters illustrates the rapid response of the ocean to wind forcing, followed by the influence of the Coriolis force in generating these anticlockwise horizontal rotary motions.

The spatial and temporal variability of NIOs is intricately linked to several key factors. Sub-inertial currents play a crucial role in modulating NIOs; weaker sub-inertial flows allow for stronger and more persistent rotary motions, while stronger sub-inertial currents can significantly deform and accelerate the decay of NIOs, thus limiting their spatial extent and vertical propagation. The thermal structure of the water column exerts a strong influence on the vertical distribution and propagation of NIOs. Warmer sea surface temperatures and stronger stratification, associated with upwelling relaxation events, favor deeper penetration of NIOs. In contrast, colder sea surface temperatures and weaker stratification, often linked to synoptic upwelling events, tend to limit the vertical extent of NIOs. This suggests that the interaction between NIOs and the thermocline plays a critical role in their propagation and energy distribution within the water column. The decay of NIOs with depth is a complex process influenced by internal wave interactions, turbulence dissipation, and advection by sub-inertial currents. The depth at which NIOs exhibit minimum velocity varies significantly, likely influenced by the dynamic interplay between these processes and the evolving thermal structure.

The presence of strong shear associated with NIOs, particularly above the thermocline, has important implications for mixing and diapycnal transport. The correlation between shear and regions of reduced stability suggests that NIOs can significantly contribute to vertical mixing within the upper ocean. Furthermore, the generation of near-inertial internal waves (NIWs) by the interaction of downward-radiating NIOs with the thermocline enhances vertical mixing and energy transfer within the water column. Local winds, especially diurnal winds intensified by sea breezes, play a crucial role in generating and modulating NIOs. The observed intensification of diurnal winds near the coast, driven by the local sea breeze, provides a significant source of energy for NIO generation. Wind relaxation events, characterized by a significant decrease in wind speed, can lead to a pronounced increase in NIO intensity due to the reduced influence of sub-inertial currents and an increased decay rate for NIOs.

The interaction between local wind-induced NIOs and background NIOs highlights the importance of advected NIOs and net circulation in the study area, which can intensify or weaken NIOs due to superposition or resonance interaction. Superposition, as the dominant interaction that intensifies net NIOs, is significantly influenced by near wind-induced NIOs that travel to location L1, where the strongest were detected at the Gulf of Arauco. The Gulf of Arauco generates a strong NIO background for Location L1, where strong NIOs travel north to interact with locally generated NIOs. Resonance and superposition between multiple NIOs and diurnal frequencies depend on the interaction between the phases of the signals. The interaction between phases could intensify or weaken NIOs; evaluating multiple phases from simulated data is a complex task due to the numerous interactions between signals involved in numerical simulations and in-situ data. A single instrument is not capable of evaluating interactions between multiple NIO frequencies, only providing the final sum of all interactions over the inertial velocity. Over the thermocline, vertical disruption of NIO velocity phases was found, which could induce significant responses in terms of superposition and resonance interaction.

Wind-induced NIOs constitute the dominant frequency in the upper ocean. We utilized inland weather stations to evaluate the relationship between NIOs and the diurnal frequency of the wind, hypothesizing a strong correlation between inland winds and those over the surface ocean at the L1 location. The first measurements of surface winds at L1 were taken in August 2024 using a weather station on-board the Posar Buoy. In-situ wind measurements at location P (Posar) during the same month were used to compare with winds from coastal weather stations, satellite data, and reanalysis wind from ERA5. These comparisons are crucial because they significantly influence the wind-induced circulation as calculated by the slab model, which employs wind stress and mixed-layer depth as primary inputs for simulating mixed-layer currents. Contrary to data from inland weather stations, where the diurnal cycle of the wind is the predominant signal in the frequency distribution, the wind data from the POSAR buoy exhibits a significant sub-diurnal signal (approximately five days). This sub-diurnal component has an energy level comparable to the diurnal frequency, making both frequencies dominant at this location. When evaluated with the slab model, mixed-layer NIOs are found to be 25% more intense using data from inland weather stations and the ERA5 reanalysis than with winds measured directly at the POSAR location. Additionally, the efficiency of energy transfer to mixed-layer currents seems higher with coastal winds from weather stations compared to the wind measurements at L1. The presence of a strong sub-inertial wind component, which is not detectable by inland weather stations, significantly modifies the wind-induced inertial oscillations in the upper ocean, highlighting the importance of localized wind measurements for accurate oceanographic modeling.

The longitudinal variability of wind drop-off significantly influences sub-diurnal wind patterns, sub-inertial wind-induced coastal circulation, and can enhance the diurnal amplitude of the wind, which is crucial for NIO generation. During summer, the fluctuations in wind drop-off interact with the along-shore intensification of the wind, driven by thermal gradients between inland coastal areas and the nearshore ocean. The strongest NIOs were observed when the sea breeze dominates the diurnal amplitude of the along-shore wind, resulting in reduced sub-inertial intensification of the geostrophic decay wind near the coast.

The interaction between NIOs and the steep bathymetry of the Chilean continental shelf is a key factor in the observed energy dissipation. The continental slope likely reflects and refracts portions of the near-inertial wave energy, leading to localized regions of enhanced mixing. This is particularly evident during periods of weak stratification, where NIOs can penetrate below the mixed layer and interact with the bottom boundary layer. The strongest NIOs at the near-bottom were detected with trajectories directed towards the coast, indicating that these NIOs could be generated over the continental slope or shelf break and travel to location L1.

Simulated Lagrangian circulation experiments at location L1, using progressive vector diagrams of current velocity, were used to release particles over the water column to evaluate the potential of NIOs to retain particles and increase the residence time in the coastal ocean. An experiment that released 100 particles per level during January 2005 indicated that NIOs have an optimal rotary trajectory to retain particles near 10-12 meters depth, where sub-inertial circulation is significant, and the effect of NIOs in retaining particles is more pronounced. In the upper ocean, strong sub-inertial velocities of the current significantly modify the rotary trajectory of NIOs, while below the mixed layer, velocities are slow, and NIOs are weak.

Our findings are consistent with previous studies documenting the generation of NIOs by strong wind forcing in coastal regions (e.g., Alford et al., 2003; D'Asaro, 1985). However, the observed trapping of NIO energy within the mixed layer during periods of strong stratification was more pronounced than in other coastal studies, likely due to the unique bathymetric and hydrographic conditions of the Chilean continental shelf. This study provides valuable insights into the generation, radiation, and impact of NIOs in the coastal ocean. However, further research is needed to quantify the impact of NIOs on

mixing and diapycnal transport, investigate mechanisms that could dramatically modify local stratification of the water column affecting NIO variability, and compare observations with high-resolution model simulations to further refine our understanding of these complex processes.

Conclusions

This study has thoroughly examined the characteristics and impacts of Near-Inertial Oscillations (NIOs) in the coastal ocean during the summer of January 2005. Our findings reveal that NIOs were the predominant feature in the current field, accounting for 63% of the variance in the horizontal velocity from 5 to 90 meters depth. These oscillations exhibited a strong anticlockwise rotary motion, particularly pronounced in the first baroclinic mode, with velocities reaching up to 8 cm/s near the surface but showing significant decay with depth. The influence of thermal structure on NIOs was evident, with stronger stratification during upwelling relaxation events allowing NIOs to penetrate deeper into the water column, while weaker stratification during upwelling events limited their vertical spread. The interaction of NIOs with sub-inertial currents was crucial; weaker sub-inertial flows supported stronger NIO rotary motions, whereas stronger sub-inertial currents led to their rapid decay. Local wind patterns, especially the diurnal winds intensified by sea breezes, played a pivotal role in NIO generation, with the Sea Breeze Index highlighting periods conducive to NIO formation. The study also identified that the decay of NIOs was modulated by the mixed-layer depth, with deeper layers allowing for longer persistence of NIOs. From a biological perspective, NIOs influenced water column properties like oxygen and fluorescence, impacting primary productivity. During strong NIO events, oxygen fluctuations were minimized in the upper ocean, suggesting a homogenization effect, while fluorescence peaks at the thermocline during relaxation phases indicated enhanced nutrient availability. Overall, this research underscores the complex interplay between physical oceanographic processes and biological activity in coastal environments, highlighting the necessity of considering NIOs for accurate modeling and understanding of coastal ocean dynamics. Further studies should focus on the long-term effects of these oscillations on marine ecosystems and the integration of high-resolution models to predict their variability and impact more accurately.

References

- Aguirre, Catalina, Oscar Pizarro, and Marcus Sobarzo. 2010. "Observations of Semidiurnal Internal Tidal Currents Off Central Chile (36.6°s)." *Continental Shelf Research* 30 (14): 1562–74. <https://doi.org/10.1016/j.csr.2010.06.003>.
- Alford, Matthew H. 2003. "Improved Global Maps and 54-Year History of Wind-Work on Ocean Inertial Motions." *Geophys. Res. Lett.* 30 (8). <https://doi.org/10.1029/2002GL016614>.
- . 2020. "(R)evisiting (n)ear-(i)nertial (w)ork: (S)lab (m)odels, (r)elative (s)tress, and (m)ixed (l)ayer (d)eepening." *Journal of Physical Oceanography* 50 (11): 3141–56. <https://doi.org/10.1175/JPO-D-20-0105.1>.
- Alford, Matthew H., Jennifer A. MacKinnon, Harper L. Simmons, and Jonathan D. Nash. 2016. "Near-Inertial Internal Gravity Waves in the Ocean." *Annu. Rev. Mar. Sci.* 8 (1): 95–123. <https://doi.org/10.1146/annurev-marine-010814-015746>.
- Arcos, Dagoberto F., and Robert E. Wilson. 1984. "Upwelling and the Distribution of Chlorophyll a Within the Bay of Concepción, Chile." *Estuarine, Coastal and Shelf Science* 18 (1): 25–35. [https://doi.org/10.1016/0272-7714\(84\)90004-0](https://doi.org/10.1016/0272-7714(84)90004-0).
- Atkison, B. W. 1995. "Sea Breeze and Local Wind. By J. E. Simpson. Cambridge University Press. 1994. Pp. 234. Price £29.95 (Hardback). ISBN 0 521 452112." *Quarterly Journal of the Royal Meteorological Society* 121 (523): 742–42. <https://doi.org/10.1002/qj.49712152315>.

- Barría, Camila, Piera Vásquez-Calderón, Catalina Lizama, Pablo Herrera, Anahi Canto, Pablo Conejeros, Orietta Beltrami, et al. 2022. "Spatial Temporal Expansion of Harmful Algal Blooms in Chile: A Review of 65 Years Records." *Journal of Marine Science and Engineering* 10 (12): 1868. <https://doi.org/10.3390/jmse10121868>.
- Chassinet, Eric P., Harley E. Hurlburt, Ole Martin Smedstad, George R. Halliwell, Patrick J. Hogan, Alan J. Wallcraft, Remy Baraille, and Rainer Bleck. 2007. "The HYCOM (HYbrid Coordinate Ocean Model) Data Assimilative System." *Journal of Marine Systems* 65 (1–4): 60–83. <https://doi.org/10.1016/j.jmarsys.2005.09.016>.
- Chen, S., D. Chen, and J. Xing. 2017. "A Study on Some Basic Features of Inertial Oscillations and Near-Inertial Internal Waves." *Ocean Science* 13 (5): 829–36. <https://doi.org/10.5194/os-13-829-2017>.
- Chen, Shengli, Xiaohui Xie, Jiuxing Xing, and Zhenyu Sun. 2019. "Near-Inertial Motions in the South China Sea." In *Regional Oceanography of the South China Sea*, 133–54. 0. WORLD SCIENTIFIC. https://doi.org/10.1142/9789811206917_0006.
- Codiga, Daniel L. 2011. "Unified Tidal Analysis and Prediction Using the UTide Matlab Functions." Graduate School of Oceanography, University of Rhode Island. <https://doi.org/10.13140/RG.2.1.3761.2008>.
- Cyriac, Ajitha, Helen E. Phillips, Nathaniel L. Bindoff, and Ming Feng. 2022. "Characteristics of Wind-Generated Near-Inertial Waves in the Southeast Indian Ocean." *Journal of Physical Oceanography* 52 (4): 557–78. <https://doi.org/10.1175/JPO-D-21-0046.1>.
- D'Asaro, Eric A. 1989. "The Decay of Wind-Forced Mixed Layer Inertial Oscillations Due to the β Effect." *J. Geophys. Res.* 94 (C2): 2045–56. <https://doi.org/10.1029/JC094iC02p02045>.
- Dai, Yanhui, Shangbo Yang, Dan Zhao, Chuanmin Hu, Wang Xu, Donald M. Anderson, Yun Li, et al. 2023. "Coastal Phytoplankton Blooms Expand and Intensify in the 21st Century." *Nature* 615 (7951): 280–84. <https://doi.org/10.1038/s41586-023-05760-y>.
- De La Maza, Lucas, and Laura Farias. 2023. "The Intensification of Coastal Hypoxia Off Central Chile: Long Term and High Frequency Variability." *Frontiers in Earth Science* 10 (January). <https://doi.org/10.3389/feart.2022.929271>.
- Delandmeter, Philippe, and Erik van Sebille. 2019. "The Parcels V2.0 Lagrangian Framework: New Field Interpolation Schemes." *Geoscientific Model Development* 12 (8): 3571–84. <https://doi.org/10.5194/gmd-12-3571-2019>.
- Du, Tianshi, Shengpeng Wang, Zhao Jing, Lixin Wu, Chao Zhang, and Bihan Zhang. 2024. "Future Changes in Coastal Upwelling and Biological Production in Eastern Boundary Upwelling Systems." *Nature Communications* 15 (1). <https://doi.org/10.1038/s41467-024-50570-z>.
- Ekman, Vagn Walfrid. 1953. *Studies on Ocean Currents: Results of a Cruise on Board the "Armauer Hansen" in 1930 Under the Leadership of Bjørn Helland-Hansen*. J. Griegs boktr., i kommisjon hos Cammermeyers boghandel.
- Escribano, Ruben, Pamela Hidalgo, Humberto González, Ricardo Giesecke, Ramiro Riquelme-Bugueno, and Karen Manríquez. 2007. "Seasonal and Inter-Annual Variation of Mesozooplankton in the Coastal Upwelling Zone Off Central-Southern Chile." *Progress in Oceanography* 75 (3): 470–85.
- Escribano, Ruben, and Wolfgang Schneider. 2007. "The Structure and Functioning of the Coastal Upwelling System Off Central/Southern Chile." *Progress in Oceanography* 75 (3): 343–47. <https://doi.org/10.1016/j.pocean.2007.08.020>.
- Farias, Laura, and Lucas de la Maza. 2024. "Understanding the Impacts of Coastal Deoxygenation in Nitrogen Dynamics: An Observational Analysis." *Scientific Reports* 14 (1). <https://doi.org/10.1038/s41598-024-62186-w>.
- Flexas, M. Mar, Andrew F. Thompson, Hector S. Torres, Patrice Klein, J. Thomas Farrar, Hong Zhang, and Dimitris Menemenlis. 2019. "Global Estimates of the Energy Transfer from the Wind to the Ocean, with Emphasis on Near-inertial

- Oscillations.” *Journal of Geophysical Research: Oceans* 124 (8): 5723–46. <https://doi.org/10.1029/2018jc014453>.
- Flinchem, E. P., and D. A. Jay. 2000. “An Introduction to Wavelet Transform Tidal Analysis Methods.” *Estuarine, Coastal and Shelf Science* 51 (2): 177–200. <https://doi.org/10.1006/ecss.2000.0586>.
- Frysinger, James R., B. Lee Lindner, and Stephen L. Brueske. 2003. “A Statistical Sea-Breeze Prediction Algorithm for Charleston, South Carolina.” *Weather and Forecasting* 18 (4): 614–25. [https://doi.org/10.1175/1520-0434\(2003\)018<0614:asspaf>2.0.co;2](https://doi.org/10.1175/1520-0434(2003)018<0614:asspaf>2.0.co;2).
- Garrett, Christopher, and Walter Munk. 1975. “Space-Time Scales of Internal Waves: A Progress Report.” *J. Geophys. Res.* 80 (3): 291–97. <https://doi.org/10.1029/JC080i003p00291>.
- Gobler, Christopher J. 2020. “Climate Change and Harmful Algal Blooms: Insights and Perspective.” *Harmful Algae* 91 (January): 101731. <https://doi.org/10.1016/j.hal.2019.101731>.
- Gregg, M. C. 1989. “Scaling Turbulent Dissipation in the Thermocline.” *J. Geophys. Res.* 94 (C7): 9686–98. <https://doi.org/10.1029/JC094iC07p09686>.
- Griffith, Andrew W., and Christopher J. Gobler. 2020. “Harmful Algal Blooms: A Climate Change Co-Stressor in Marine and Freshwater Ecosystems.” *Harmful Algae* 91 (January): 101590. <https://doi.org/10.1016/j.hal.2019.03.008>.
- Hallegraeff, Gustaaf, Henrik Enevoldsen, and Adriana Zingone. 2021. “Global Harmful Algal Bloom Status Reporting.” *Harmful Algae* 102 (February): 101992. <https://doi.org/10.1016/j.hal.2021.101992>.
- Holte, James, and Lynne Talley. 2009. “A New Algorithm for Finding Mixed Layer Depths with Applications to Argo Data and Subantarctic Mode Water Formation.” *Journal of Atmospheric and Oceanic Technology* 26 (9): 1920–39. <https://doi.org/10.1175/2009JTECHO543.1>.
- Johnston, T. M. Shaun, Dipanjan Chaudhuri, Manikandan Mathur, Daniel L. Rudnick, Debasis Sengupta, Harper L. Simmons, Amit Tandon, and R. Venkatesan. 2016. “Decay Mechanisms of Near-Inertial Mixed Layer Oscillations in the Bay of Bengal.” *Oceanography* 29 (2): 180–91. <http://www.jstor.org/stable/24862681>.
- Kelly, Samuel M. 2019. “Coastally Generated Near-Inertial Waves.” *Journal of Physical Oceanography* 49 (11): 2979–95. <https://doi.org/10.1175/JPO-D-18-0148.1>.
- Kunze, Eric, Melbourne G. Briscoe, and A. J. Williams III. 1990. “Interpreting Shear and Strain Fine Structure from a Neutrally Buoyant Float.” *J. Geophys. Res.* 95 (C10): 18111–25. <https://doi.org/10.1029/JC095iC10p18111>.
- Large, W. G., and S. Pond. 1981. “Open Ocean Momentum Flux Measurements in Moderate to Strong Winds.” *Journal of Physical Oceanography* 11 (3): 324–36. [https://doi.org/10.1175/1520-0485\(1981\)011<0324:oomfmi>2.0.co;2](https://doi.org/10.1175/1520-0485(1981)011<0324:oomfmi>2.0.co;2).
- Lilly, Jonathan M. 2017. “Element Analysis: A Wavelet-Based Method for Analysing Time-Localized Events in Noisy Time Series.” *Proceedings of the Royal Society A: Mathematical, Physical and Engineering Sciences* 473 (2200): 20160776. <https://doi.org/10.1098/rspa.2016.0776>.
- Lilly, Jonathan M., and Sofia C. Olhede. 2010. “On the Analytic Wavelet Transform.” *IEEE Transactions on Information Theory* 56 (8): 4135–56. <https://doi.org/10.1109/tit.2010.2050935>.
- Liu, Yongzheng, Zhao Jing, and Lixin Wu. 2019. “Wind Power on Oceanic Near-Inertial Oscillations in the Global Ocean Estimated from Surface Drifters.” *Geophys. Res. Lett.* 46 (5): 2647–53. <https://doi.org/10.1029/2018GL081712>.
- Melton, Christopher, Libe Washburn, and Chris Gotschalk. 2009. “Wind Relaxations and Poleward Flow Events in a Coastal Upwelling System on the Central California Coast.” *J. Geophys. Res.* 114 (C11). <https://doi.org/10.1029/2009JC005397>.
- Oyarzún, Damián, and Chris M. Brierley. 2018. “The Future of Coastal Upwelling in the Humboldt Current from Model Projections.” *Climate Dynamics* 52 (1–2): 599–615. <https://doi.org/10.1007/s00382-018-4158-7>.

- Pollard, R. T., and R. C. Millard. 1970. "Comparison Between Observed and Simulated Wind-Generated Inertial Oscillations." *Deep Sea Research and Oceanographic Abstracts* 17 (4): 813–21. [https://doi.org/10.1016/0011-7471\(70\)90043-4](https://doi.org/10.1016/0011-7471(70)90043-4).
- Qian, Jiangchao, Xiaoming Zhai, Zhaomin Wang, and Markus Jochum. 2023. "Distribution and Trend of Wind Power Input to Near-inertial Motions in the Southern Ocean." *Geophysical Research Letters* 50 (18). <https://doi.org/10.1029/2023gl105411>.
- Raja, Keshav J., Maarten C. Buijsman, Jay F. Shriver, Brian K. Arbic, and Oladeji Siyanbola. 2022. "Near-Inertial Wave Energetics Modulated by Background Flows in a Global Model Simulation." *Journal of Physical Oceanography* 52 (5): 823–40. <https://doi.org/10.1175/jpo-d-21-0130.1>.
- Sobarzo, Marcus, Luis Bravo, and Carlos Moffat. 2010. "Diurnal-Period, Wind-Forced Ocean Variability on the Inner Shelf Off Concepción, Chile." *Continental Shelf Research* 30 (20): 2043–56. <https://doi.org/10.1016/j.csr.2010.10.004>.
- Sobarzo, Marcus, and Leif Djurfeldt. 2004. "Coastal Upwelling Process on a Continental Shelf Limited by Submarine Canyons, Concepción, Central Chile." *Journal of Geophysical Research: Oceans* 109 (C12). <https://doi.org/10.1029/2004jc002350>.
- Sobarzo, Marcus, R. Kipp Shearman, and Steve Lentz. 2007. "Near-Inertial Motions over the Continental Shelf Off Concepción, Central Chile." *Progress in Oceanography* 75 (3): 348–62. <https://doi.org/10.1016/j.pocean.2007.08.021>.
- Song, Dehai, Guandong Gao, Yingying Xia, Zhaopeng Ren, Junliang Liu, Xianwen Bao, and Baoshu Yin. 2021. "Near-Inertial Oscillations in Seasonal Highly Stratified Shallow Water." *Estuarine, Coastal and Shelf Science* 258: 107445. <https://doi.org/10.1016/j.ecss.2021.107445>.
- Tintoré, J., D.-P. Wang, E. García, and A. Viúdez. 1995. "Near-Inertial Motions in the Coastal Ocean." *Journal of Marine Systems* 6 (4): 301–12. [https://doi.org/10.1016/0924-7963\(94\)00030-F](https://doi.org/10.1016/0924-7963(94)00030-F).
- Wang, Jinbo, Hector Torres, Patrice Klein, Alexander Wineteer, Hong Zhang, Dimitris Menemenlis, Clement Ubelmann, and Ernesto Rodriguez. 2023. "Increasing the Observability of Near Inertial Oscillations by a Future ODYSEA Satellite Mission." *Remote Sensing* 15 (18). <https://doi.org/10.3390/rs15184526>.
- Watanabe, M., and T. Hibiya. 2002. "Global Estimates of the Wind-Induced Energy Flux to Inertial Motions in the Surface Mixed Layer." *Geophys. Res. Lett.* 29: 1239. <https://doi.org/10.1029/2001GL014422>.
- Webster, Ferris. 1968. "Observations of Inertial-Period Motions in the Deep Sea." *Rev. Geophys.* 6 (4): 473–90. <https://doi.org/10.1029/RG006i004p00473>.
- Xing, Jiuxing, and Alan M. Davies. 2004. "On the Influence of a Surface Coastal Front on Near-inertial Wind-induced Internal Wave Generation." *Journal of Geophysical Research: Oceans* 109 (C1). <https://doi.org/10.1029/2003jc001794>.